

## RESEARCH ARTICLE

## Plxdc family members are novel receptors for the rhesus monkey rhadinovirus (RRV)

Anna K. Großkopf<sup>1</sup>, Sarah Schlagowski<sup>1</sup>, Thomas Fricke<sup>1</sup>, Armin Ensser<sup>2</sup>, Ronald C. Desrosiers<sup>3</sup>, Alexander S. Hahn<sup>1\*</sup>

**1** German Primate Center - Leibniz Institute for Primate Research, Göttingen, Germany,

**2** Universitätsklinikum Erlangen, Institute for Clinical and Molecular Virology, Erlangen, Germany, **3** Miller School of Medicine, University of Miami, Miami, United States of America

\* [ahahn@dpz.eu](mailto:ahahn@dpz.eu)



## OPEN ACCESS

**Citation:** Großkopf AK, Schlagowski S, Fricke T, Ensser A, Desrosiers RC, Hahn AS (2021) Plxdc family members are novel receptors for the rhesus monkey rhadinovirus (RRV). *PLoS Pathog* 17(3): e1008979. <https://doi.org/10.1371/journal.ppat.1008979>

**Editor:** Zhi-Ming Zheng, National Cancer Institute, UNITED STATES

**Received:** September 17, 2020

**Accepted:** February 4, 2021

**Published:** March 3, 2021

**Copyright:** © 2021 Großkopf et al. This is an open access article distributed under the terms of the [Creative Commons Attribution License](https://creativecommons.org/licenses/by/4.0/), which permits unrestricted use, distribution, and reproduction in any medium, provided the original author and source are credited.

**Data Availability Statement:** All relevant data are within the manuscript and its [Supporting information](#) files.

**Funding:** This work was supported by grants to A.S.H. from the Deutsche Forschungsgemeinschaft ([www.dfg.de](https://www.dfg.de), HA 6013/1, HA 6013/4-1), the Wilhelm-Sander Foundation ([www.wilhelm-sander-stiftung.de](https://www.wilhelm-sander-stiftung.de), project 2019.027.1), and the Interdisciplinary Center for Clinical Research Erlangen (IZKF, [www.izkf.med.fau.de](https://www.izkf.med.fau.de), grant J44), by the Deutsche Forschungsgemeinschaft ([www.dfg.de](https://www.dfg.de)).

## Abstract

The rhesus monkey rhadinovirus (RRV), a  $\gamma$ 2-herpesvirus of rhesus macaques, shares many biological features with the human pathogenic Kaposi's sarcoma-associated herpesvirus (KSHV). Both viruses, as well as the more distantly related Epstein-Barr virus, engage cellular receptors from the Eph family of receptor tyrosine kinases (Ephs). However, the importance of the Eph interaction for RRV entry varies between cell types suggesting the existence of Eph-independent entry pathways. We therefore aimed to identify additional cellular receptors for RRV by affinity enrichment and mass spectrometry. We identified an additional receptor family, the Plexin domain containing proteins 1 and 2 (Plxdc1/2) that bind the RRV gH/gL glycoprotein complex. Preincubation of RRV with soluble Plxdc2 decoy receptor reduced infection by ~60%, while overexpression of Plxdc1 and 2 dramatically enhanced RRV susceptibility and cell-cell fusion of otherwise marginally permissive Raji cells. While the Plxdc2 interaction is conserved between two RRV strains, 26–95 and 17577, Plxdc1 specifically interacts with RRV 26–95 gH. The Plxdc interaction is mediated by a short motif at the N-terminus of RRV gH that is partially conserved between isolate 26–95 and isolate 17577, but absent in KSHV gH. Mutation of this motif abrogated the interaction with Plxdc1/2 and reduced RRV infection in a cell type-specific manner. Taken together, our findings characterize Plxdc1/2 as novel interaction partners and entry receptors for RRV and support the concept of the N-terminal domain of the gammaherpesviral gH/gL complex as a multifunctional receptor-binding domain. Further, Plxdc1/2 usage defines an important biological difference between KSHV and RRV.

## Author summary

KSHV is the causative agent of a group of malignancies which account for a substantial disease burden in particular in sub-Saharan Africa. RRV, a related virus of rhesus macaques, has shown promise as model system for KSHV and for the development of immunization strategies. To exploit the full potential of the RRV animal model system, detailed knowledge of commonalities and differences between KSHV and RRV is key. Here, we describe the Plexin domain containing proteins 1 and 2 as a novel receptor

dfg.de), grants CRC 796, TP B1 and EN423/5-1 to A.E., by a grant to A.E. from the Interdisciplinary Center for Clinical Research Erlangen (IZKF, [www.izkf.med.fau.de](http://www.izkf.med.fau.de), grant A81), by grant R01 AI072004 from the National Institutes of Health (NIH, [www.nih.gov](http://www.nih.gov)) to R.C.D., and by base grant RR00168 from the NIH ([www.nih.gov](http://www.nih.gov)) to the New England Primate Research Center. The funders had no role in study design, data collection and analysis, decision to publish, or preparation of the manuscript.

**Competing interests:** The authors have declared that no competing interests exist.

family which mediates entry of RRV, but not of KSHV. Infection experiments using RRV mutants deleted of the Plxdc interaction motif suggest a cell type-specific contribution of Plxdc receptors to RRV infection. As information on Plxdc1/2 and its biological function is still sparse, analysis of the RRV–Plxdc interaction will help to characterize the physiological and pathophysiological role of this receptor family.

## Introduction

The rhesus monkey rhadinovirus (RRV), a member of the genus  $\gamma$ 2-herpesvirus or rhadinovirus, is closely related to the only human pathogenic member of this genus, the Kaposi's sarcoma-associated herpesvirus (KSHV) [1,2]. Due to the high similarity in both genome organization and biology RRV is considered as an animal model virus for KSHV [3] and has been used as such in *in vitro* and *in vivo* studies. Two major RRV sequence groups have been identified [4], and each is represented by a cloned isolate, RRV 26–95 [5] and RRV 17577 [6]. Analogous to KSHV infection, primary RRV infection is asymptomatic in healthy hosts and leads to life-long persistence, most likely in the B cell compartment [7].

KSHV is associated with a solid tumor of endothelial origin, Kaposi's sarcoma (KS), and two B cell malignancies, primary effusion lymphoma (PEL) and the plasmablastic variant of multicentric Castleman's disease (MCD), most prominently in the context of human immunodeficiency virus (HIV) infection and in immunocompromised individuals. Similarly, simian immunodeficiency virus (SIV)-positive rhesus macaques developed B cell lymphomas upon experimental infection with RRV strain 17577 [8,9] and several studies correlated RRV infection with lymphomagenesis in SIV/SHIV-infected animals [10,11]. While RRV is not consistently associated with solid malignancies, RRV has been identified in retroperitoneal fibromatosis tissue [9,12], similar to retroperitoneal fibromatosis herpesvirus (RFHV)[11], and was recently isolated from hemangioma tissue [13].

Another shared characteristic of KSHV and RRV is the receptor usage on a range of cell types. Both viruses engage members of the Eph family of receptor tyrosine kinases (Ephs) through their glycoprotein (g)H/gL complex to facilitate entry into target cells. While KSHV preferentially interacts with A-type Ephs—specifically EphA2 as the high affinity receptor [14,15]—RRV can utilize both A- and B-type Ephs [15] for entry. These interactions have been characterized on different adherent cells types [16–19] and we could recently show that both viruses can utilize EphA7 as receptor on BJAB cells [20], a model B lymphocyte line. While for KSHV, in addition to Eph family receptors, several membrane proteins have been proposed as cellular receptors for different viral glycoproteins mediating either attachment or entry on a range of target cells (reviewed in [21]) the receptor usage of RRV is comparatively less well characterized. Nevertheless, studies using receptor knock-down or knockout [14,22], receptor- and ligand-mediated blocking [15,23], and Eph de-targeted virus mutants [23,24] showed that both viruses and in particular RRV can infect various cells partially or completely independently of the Eph-interaction, which suggests that RRV engages at least one additional entry receptor that can functionally substitute for the Eph-interaction. This notion is also supported by a recent *in vivo* study that demonstrated that an RRV mutant deleted of gL and therefore unable to interact with Eph receptors still establishes persistent infection in RRV-naïve rhesus macaques upon intravenous inoculation [24].

We therefore aimed to identify additional rhadinovirus receptors that bind the gH/gL complex or gH and identified Plexin domain containing protein 2 (Plxdc2) as novel interaction partner of the gH/gL complex of RRV, but not KSHV. The closest homolog to Plxdc2, Plxdc1

was initially identified as overexpressed in blood vessels of solid human tumors [25], resulting in the original terminology tumor endothelial marker 7 (TEM7, Plxdc1) and tumor endothelial marker 7 related (TEM7R, Plxdc2) [26]. In general, the physiological functions of Plxdc1/2 are not well understood. Suggestive of a role in development, Plxdc2 has been described as mitogen for neural progenitor cells [27] and expression of both Plxdc1 and Plxdc2 in the developing nervous system has been demonstrated [28,29]. Cortactin, nidogen and the pigment epithelium-derived factor (PEDF) have been described as interactors for Plxdc1 and Plxdc2 [30–32]. However, the physiological relevance of these interactions is not fully understood. In this study we characterized the interaction of Plxdc1/2 with the gH/gL glycoprotein complex of RRV and establish Plxdc1/2 as novel cellular RRV entry receptors.

**Results**

To identify potential cellular receptors for RRV glycoprotein H, we performed immunoprecipitation using soluble RRV 26–95 gH, consisting of the extracellular part fused to the Fc part of human IgG (RRV gH-FcStrep) as bait and 293T whole cell lysate as prey (Fig 1A). Bands

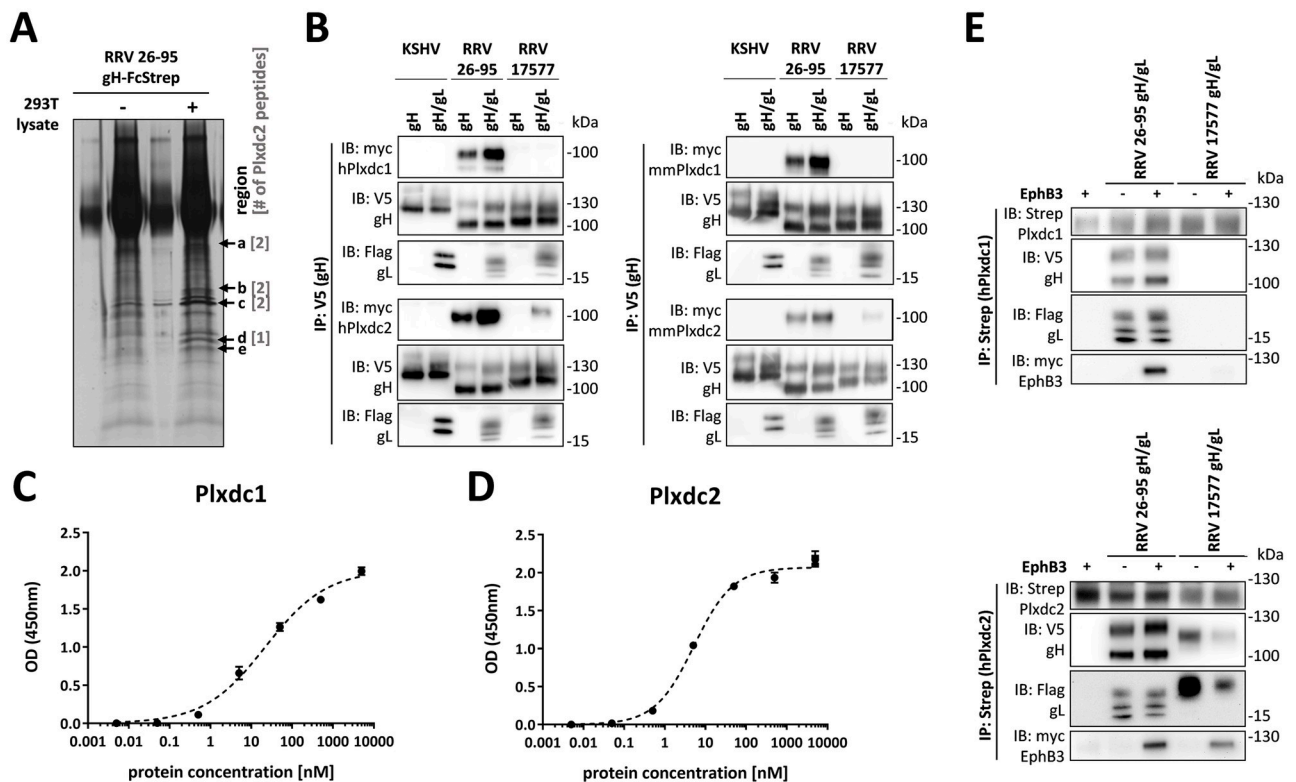


**Fig 1. Plxdc family receptors are novel interaction partners for RRV gH/gL.** A) Immunoprecipitation of recombinant soluble RRV 26–95 gH-FcStrep in the presence or absence of 293T lysate. Precipitates were analyzed by PAGE, silver stained and bands at the indicated molecular weight (arrows, regions a-e) were excised and analyzed by mass spectrometry. Numbers in brackets indicate the number of Plxdc2 peptides identified by LC-MS/MS in each region. B) V5-tagged RRV 26–95 gH, RRV 17577 gH or KSHV gH alone or co-expressed with the respective Flag-tagged gL construct were immunoprecipitated in the presence of full-length Plxdc1 or Plxdc2 of human (h) or *Macaca mulatta* (mm) origin using monoclonal antibody to the V5-tag. Precipitates were analyzed by Western blot with the indicated antibodies. C-D) Binding of Plxdc1 ectodomain C) or Plxdc2 ectodomain D) at various concentrations to immobilized RRV 26–95 gH-FcStrep/gL was measured by enzyme-linked immunosorbent assay. Curve fitting and determination of half-maximal binding concentration was performed based on the *One site specific binding with Hill Slope equation* in Prism6. E) Co-immunoprecipitation of soluble human Plxdc1-FcStrep or human Plxdc2-FcStrep with RRV 26–95 gH-V5/gL-Flag or RRV 17577 gH-V5/gL-Flag using StrepTactin sepharose in the presence or absence of human full-length myc-tagged EphB3. Abbreviations: IP: immunoprecipitation, IB: immunoblotting, h: human, mm: *Macaca mulatta* (rhesus macaque).

<https://doi.org/10.1371/journal.ppat.1008979.g001>

present in the precipitation from 293T whole cell lysate, but not in control precipitation without 293T lysate were excised and analyzed by LC-MS/MS. The most abundant cell surface protein, identified in four of the five analyzed regions, was Plxdc2, also known as TEM7R, a cellular transmembrane protein. Plxdc1/TEM7, the only homolog of Plxdc2 in humans and rhesus macaques, was not detected in our mass spectrometry analysis (see [S1 Table](#) for a list of peptides identified by LC-MS/MS). This may be explained by the low expression levels of Plxdc1 in 293T cells suggested by previously published RNAseq data ([S1A Fig](#)) and confirmed by real-time PCR (qPCR) analysis of our 293T cells ([S1B Fig](#)). Plxdc1 was therefore included in subsequent analyses. Human and rhesus Plxdc1 (ref |NM\_020405.5|; ref |XM\_028836436.1|) and Plxdc2 (ref |NM\_032812.9|; ref |XM\_028826043.1|) are 96.80% and 97.92% identical on the amino sequence level, while Plxdc1 and Plxdc2 of human and rhesus origin share 57.34% and 56.04% sequence identity, respectively (for complete alignment and domain junctions see [S1C Fig](#)).

Co-immunoprecipitation of V5-tagged expression constructs of gH from KSHV and from the two RRV isolates 26–95 and 17577, in the presence or absence of the corresponding Flag-tagged gL proteins with myc-tagged human or rhesus Plxdc1 or Plxdc2 (hPlxdc1-myc/hPlxdc2-myc/mmPlxdc1-myc/mmPlxdc2-myc) from transfected 293T cells confirmed the interaction of both RRV gH/gL complexes with Plxdc2 ([Fig 1B](#)). While the predicted molecular weight of Plxdc1 and Plxdc2 is 56kDa and 60kDa, respectively, we and others detect Plxdc1/2 at an apparent molecular weight of ~100kDa [31]. Neither KSHV gH/gL nor RRV 17577 gH/gL interacted detectably with Plxdc1-myc, while RRV 26–95 prominently bound both Plxdc1 and Plxdc2 in the presence and absence of gL. Measurement of the binding of purified hPlxdc1 and hPlxdc2 ectodomain to immobilized RRV 26–95 gH-FcStrep/gL by enzyme-linked immunosorbent assay ([Fig 1C and 1D](#)) showed a half-maximal binding concentration of 22.2nM for Plxdc1 and 5.2nM for Plxdc2 as calculated for one site specific binding without pre-defined Hill slope.

To evaluate the effect of Plxdc-binding to RRV gH on the interaction with EphB3, the high-affinity Eph family receptor for RRV gH/gL [15], we used soluble human Plxdc1 or Plxdc2, consisting of the extracellular part of Plxdc1 or Plxdc2 fused to the Fc part of human IgG followed by a TwinStrep tag (hPlxdc1-FcStrep/hPlxdc2-FcStrep) in immunoprecipitation experiments. Co-immunoprecipitation of hPlxdc1-FcStrep/hPlxdc2-FcStrep with the gH-V5/gL-Flag complexes of RRV isolates 26–95 and 17577 in the presence or absence of myc-tagged EphB3 from transfected 293T cells demonstrated the existence of a quaternary complex, indicating the ability of RRV gH/gL to interact with members of both receptor families simultaneously. As the complex was precipitated via Strep-tagged Plxdc1 or Plxdc2 –and Plxdc1/2 alone do not interact with EphB3 –EphB3 will only be co-precipitated when a complex between RRV gH/gL and both EphB3 and Plxdc1 or Plxdc2 is formed ([Fig 1E](#)).

While interaction of purified proteins and in transfected cell lysates is strongly suggestive of a functional interaction, the biologically relevant interaction for the entry process would occur with virion gH/gL. To evaluate the functionality of the gH/gL-Plxdc interaction on virus particles both for wildtype RRV and an Eph-binding-negative RRV mutant, we utilized RRV-YFP, an RRV 26–95 strain engineered for constitutive YFP expression upon infection, and RRV-YFP gH-AELAAN, an Eph-binding-negative RRV-YFP mutant that we had previously described ([Fig 2A](#)) [23]. To analyze the impact of competition with soluble Plxdc decoy receptor, RRV-YFP wt and RRV-YFP gH-AELAAN preparations were incubated with a concentration series of soluble hPlxdc2-FcStrep or an FcStrep control prior to infection of HaCaT cells ([Fig 2B](#)). According to RNA-Seq data of 36 cell lines (courtesy of Human Protein Atlas, [www.proteinatlas.org](http://www.proteinatlas.org) [33], retrieved 2020), HaCaT cells exhibit the highest cell-line specific expression of Plxdc2 among the analyzed non-cancer cell lines and were therefore chosen for further

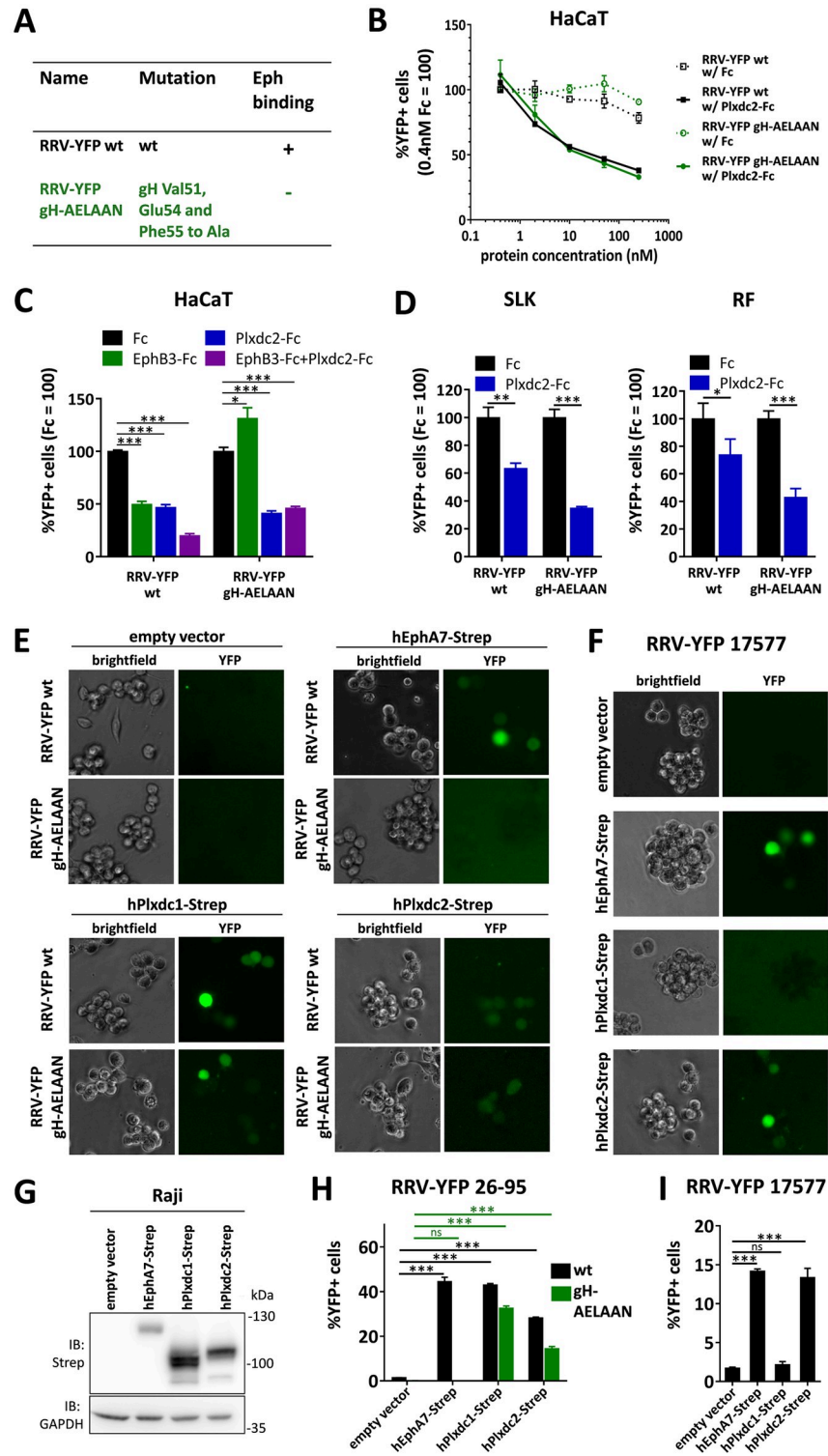


**Fig 2. Plxdc1/2 function as entry receptors for RRV.** A) List of BAC-derived recombinant viruses and introduced mutations used in this figure. B) Dose-dependent inhibition of RRV 26–95 infection by soluble human Plxdc2-FcStrep on HaCaT cells. RRV-YFP wt and RRV-YFP gH-AELAAN were pre-incubated with hPlxdc2-FcStrep for 30min at room temperature. FcStrep alone was used as control. YFP expression as indicator of infection was measured by flow cytometry. Infection in the presence of 0.4nM FcStrep was set to 100% (MOI ~0.2, triplicates, error bars represent SD). C) Inhibition of RRV 26–95 infection by soluble Plxdc2-FcStrep and EphB3-Fc on HaCaT cells. RRV-YFP wt and RRV-YFP gH-AELAAN were pre-incubated with 100nM hPlxdc2-FcStrep, 10nM EphB3-Fc or a combination of 100nM hPlxdc2-FcStrep and 10nM EphB3-Fc for 30min at room temperature. FcStrep alone was used as control. YFP

expression as indicator of infection was measured by flow cytometry. Infection with FcStrep was set to 100% (MOI ~0.2, triplicates, error bars represent SD). **D**) Inhibition of RRV 26–95 infection by soluble human Plxdc2-FcStrep on SLK cells and rhesus monkey fibroblasts (RF). RRV-YFP wt and RRV-YFP gH-AELAAN were pre-incubated with 250nM hPlxdc2-FcStrep for 30min at room temperature. FcStrep alone was used as control. YFP expression as indicator of infection was measured by flow cytometry. Infection with FcStrep was set to 100% (MOI ~0.05–0.1, triplicates, error bars represent SD). **E–F**) Raji cells were transduced with TwinStrep-tagged human Plxdc1, Plxdc2 or EphA7 (hPlxdc1-Strep/ hPlxdc2-Strep/ hEphA7-Strep) expression constructs or an empty vector control, briefly selected and infected with RRV-YFP 26–95 wt and RRV-YFP 26–95 gH-AELAAN (**E**) or RRV-YFP 17577 (**F**) normalized to genome copies as determined by qPCR. Micrographs show representative infection of the indicated cell pools. **G**) Lysates of transduced Raji cell pools were analyzed for EphA7-Strep and Plxdc1/2-Strep expression by Western blot. **H**) Quantification of (**E**) by flow cytometric analyses of YFP reporter gene expression as indicator of infection (triplicates, error bars represent SD). **I**) Quantification of (**F**) by flow cytometric analyses of YFP reporter gene expression as indicator of infection (triplicates, error bars represent SD).

<https://doi.org/10.1371/journal.ppat.1008979.g002>

analyses. Soluble hPlxdc2-FcStrep inhibited RRV-YFP wt infection up to ~60% in a dose dependent manner when compared to FcStrep alone. Likewise, preincubation of RRV-YFP gH-AELAAN with hPlxdc2-FcStrep reduced infection by ~65%. RRV-YFP wt and RRV-YFP gH-AELAAN infection was normalized to ~MOI 0.2. In a side by side comparison, inhibition of the gH/gL-Eph interaction, which served as control, lead to an ~50% reduction of RRV-YFP wt infection at a concentration of 10nM hEphB3-Fc while 100nM of soluble hPlxdc2-FcStrep exhibited a similar blocking efficiency (**Fig 2C**, left column group). Preincubation with both hEphB3-Fc and hPlxdc2-FcStrep further reduced RRV-YFP wt infection on HaCaT cells, when compared to preincubation with either hEphB3-Fc or hPlxdc2-FcStrep alone (**Fig 2C**, left column group). While preincubation with EphB3-Fc did not reduce RRV-YFP gH-AELAAN infection, preincubation with either hPlxdc2-FcStrep or a combination of hPlxdc2-FcStrep and hEphB3-Fc reduced infection by ~50% as observed for RRV-YFP wt infection (**Fig 2C**, right column group). Infection of SLK cells and rhesus monkey fibroblasts (RF) was also slightly decreased by preincubation of the viral inoculum with hPlxdc2-FcStrep, infection of SLK by RRV-YFP wt to 63.5% ± 3.7% and infection of RF by RRV-YFP wt to 73.9% ± 11.3% relative to preincubation with FcStrep as control. However, this effect was less pronounced than on HaCaT and less pronounced than the effect of hPlxdc2-FcStrep on RRV-YFP gH-AELAAN infection of the same cell types (**Fig 2D**). Taken together, the immunoprecipitation and blocking experiments confirm the independence of the gH-Plxdc interaction of the previously described Eph interaction motif [23] and EphB3-binding.

To establish receptor function, we performed gain-of-function experiments using ectopic Plxdc1/2 overexpression (**Fig 2E–2I**). Raji cells were transduced with lentiviruses encoding TwinStrep-tagged human Plxdc1/2 constructs (hPlxdc1-Strep/ hPlxdc2-Strep). A TwinStrep-tagged human EphA7 construct (hEphA7-Strep) was used as control for Eph-mediated RRV infection (**Fig 2G**). The EBV-positive, human lymphoblast cell line only allows for low-level RRV 26–95 infection even with amounts of input virus corresponding to high MOI on adherent cells like SLK, HaCaT or RF. Therefore, changes in susceptibility to infection mediated by Plxdc1/2 overexpression should be readily detectable and allow for a clear differentiation of the contribution of Plxdc1/2 to RRV infection over the very low intrinsic susceptibility to infection. Indeed, ectopic expression of both hPlxdc1- and hPlxdc2-Strep dramatically increased RRV-YFP 26–95 wt infection from ~1.4% basal infection to 42.9% and 28.2% infection, respectively (**Fig 2E and 2H**). Similarly, RRV-YFP gH-AELAAN infection was increased from 0.04% on empty vector-transduced cells to 32.5% and 14.4% on cells transduced with constructs encoding hPlxdc1-Strep and hPlxdc2-Strep, respectively. EphA7, which had previously been described by our group to be critical for RRV infection of BJAB B lymphocytes enhanced RRV-YFP wt infection to 44.4% while infection with the Eph-binding-negative mutant RRV-YFP gH-AELAAN was not affected (**Fig 2E and 2H**). We did not observe

pronounced differences in RRV-YFP 26–95 infection mediated by hPlxdc1-Strep or hPlxdc2-Strep, indicating no clear Plxdc receptor preference of RRV 26–95. RRV-YFP 17577 infection was increased 8.4-fold upon recombinant expression of hEphA7-Strep and 7.9-fold upon recombinant expression of hPlxdc2-Strep, but remained unaffected by hPlxdc1-Strep expression (Fig 2F and 2I). Taken together, the observed receptor usage on hPlxdc1/2-Strep-overexpressing Raji cells by RRV-YFP 26–95 and RRV-YFP 17577 reflects the Plxdc1/2 interaction patterns of RRV 26–95 and RRV 17577 gH/gL complexes observed in immunoprecipitation experiments (Fig 1B).

In a next step we characterized the Plxdc binding motif on RRV gH. As the RRV 17577 gH-Plxdc2 interaction depends on gL whereas the RRV 26–95 gH-Plxdc2 interaction does not, we focused on the N-terminal domain I of gH which, in analogy to EBV gH/gL [34], most likely constitutes the gL-binding interface. The differences in the Plxdc interaction of RRV isolates 26–95 and 17577 as well as the lack of an interaction between KSHV gH/gL and Plxdc receptors suggested a motif that is only partially conserved between the RRV isolates and missing in KSHV. Using sequence comparisons (Fig 3A) we identified a putative interaction motif spanning 7 or 6 amino acid motif in the N-terminal region of RRV 26–95 gH and RRV 17577 gH, respectively, that is not conserved in KSHV gH. The motif is located close to the Eph-interaction motif we described previously, facing in the opposite direction in a homology model of the RRV 26–95 gH/gL complex based on the EBV gH/gL crystal structure (3PHF) (Fig 3B). Deletion of this motif completely abrogated the interaction with Plxdc2 of both RRV 26–95 gH (Fig 3C) and RRV 17577 gH/gL (Fig 3D). To further characterize the contribution of individual residues in the ‘Tyr(Y)-Glu(E)-Tyr(Y)-Asn(N)-Glu(E)-Glu(E)-Lys(K)’ (RRV 26–95) motif we performed single amino acid substitutions to alanine. The ability of mutant RRV 26–95 gH-V5 to bind myc-tagged Plxdc1/2 of human (hPlxdc1/2-myc) (Fig 3E) or rhesus macaque origin (mmPlxdc1/2-myc) (Fig 3F) was analyzed by immunoprecipitation of gH via the V5-tag and Western blot. While several single amino acid substitutions decreased the interaction of RRV gH with Plxdc2 to some degree, residues Tyr23 and Glu25 that are conserved in isolates 26–95 and 17577 appear to be critical for the interaction of gH with human and rhesus macaque Plxdc1 and Plxdc2. Furthermore, substitution of glutamate with alanine at position 22, which is not conserved between isolates 26–95 and 17577, had a pronounced, albeit slightly weaker effect on the gH-Plxdc1/2 interaction (Fig 3E and 3F).

To further analyze the contribution of the gH/gL-Plxdc interaction in the context of infection we constructed virus mutants deleted in the seven amino acid interaction motif in the background of RRV-YFP 26–95 wildtype (RRV-YFP gH $\Delta$ 21–27), and in the background of an RRV-YFP 26–95 strain mutated in the Eph-interaction motif described previously by our group (RRV-YFP gH-AELAAN, RRV-YFP gH $\Delta$ 21–27-AELAAN) using a two-step, lambda red-mediated recombination system [35] (Fig 4A). Blocking experiments using soluble hPlxdc2-FcStrep decoy receptor on HaCaT cells confirmed that deletion of the seven amino acid motif was sufficient to abrogate the gH-Plxdc2 interaction on viral particles (Fig 4B). While infection of RRV-YFP wt and RRV-YFP gH-AELAAN was inhibited by ~60% and 70% respectively, infection of RRV-YFP gH $\Delta$ 21–27 and RRV-YFP gH $\Delta$ 21–27-AELAAN was not affected even by high concentrations of soluble hPlxdc2-FcStrep (Fig 4B). All infections were carried out at ~MOI 0.05. Analogously, the Eph- or Plxdc-receptor-binding-negative RRV mutants were no longer inhibited by preincubation with the respective soluble receptor (hEphB3-Fc or hPlxdc2-FcStrep) in single or double inhibition experiments on HaCaT cells (Fig 4C). To analyze the direct effect of interference with Plxdc receptors on the cellular side for RRV infection we performed an siRNA mediated knock-down of Plxdc2 (S2 Fig). We choose 293T cells for their high transfection efficiency and confirmed Plxdc2 expression by qPCR, in accordance with our initial mass spectrometry experiment (Fig 1A and S1 Fig). The



or Plxdc2-myc using monoclonal antibody to the V5-tag. Precipitates were analyzed by Western blot. RRV gH $\Delta$ 21–27 serves as negative control. F) Mutational scan of the Plxdc interaction motif (amino acid 21–27, “YEYNEEK”) of RRV 26–95 gH identifies rhesus macaque Plxdc1/2-interacting residues. V5-tagged gH mutants were immunoprecipitated in the presence of full-length *Macaca mulatta* Plxdc1-myc or Plxdc2-myc using monoclonal antibody to the V5-tag. Precipitates were analyzed by Western blot. RRV gH $\Delta$ 21–27 serves as negative control. Abbreviations: IP: immunoprecipitation, IB: immunoblotting, h: human, mm: *Macaca mulatta* (rhesus macaque).

<https://doi.org/10.1371/journal.ppat.1008979.g003>

~50% decrease in Plxdc2 mRNA levels upon transfection of a set of 4 siRNAs directed against Plxdc2 (S2A Fig) resulted in a small ( $17.6\% \pm 0.02\%$ ) but significant decrease in RRV-YFP gH-AELAAN infection compared to siCtrl transfected cells, which was consistent using two different RRV stocks in two virus dilutions each (S2B and S2C Fig). Control infection with Plxdc-detargeted RRV mutants (RRV-YFP gH $\Delta$ 21–27, RRV-YFP gH $\Delta$ 21–27-AELAAN) was not affected. Similarly, knock-down of Plxdc2 alone did not lead to a decrease in RRV-YFP wt infection, which is probably explained by the expression of a multitude of Eph family receptors on 293T and relatively weak knockdown (S1A and S2A Figs). We next performed antibody mediated blocking experiments using two custom made polyclonal rabbit sera (SY8512, SY8513) raised against recombinant Plxdc2-FcStrep on 293T cells (S2D–S2F Fig). Compared to pre-immune sera from the same rabbits, serum SY8512 lead to a  $41.3\% \pm 2.8\%$  reduction in RRV-YFP wt infection and a  $60.0\% \pm 3.1\%$  reduction in RRV-YFP gH-AELAAN infection, while infection with RRV-YFP gH $\Delta$ 21–27 and RRV-YFP gH $\Delta$ 21–27-AELAAN was not significantly affected (S2D Fig). Similarly, serum SY8513 reduced RRV-YFP wt and RRV-YFP gH-AELAAN infection by  $34.6\% \pm 1.6\%$  and  $40.0\% \pm 5.7\%$  compared to pre-immune serum. While pre-treatment of 293T cells with serum SY8513 did not significantly affect infection with RRV-YFP gH $\Delta$ 21–27, it lead to a  $30.6\% \pm 6.9\%$  reduction of infection with the Plxdc-binding negative RRV-YFP gH $\Delta$ 21–27-AELAAN (S2E Fig). Overall, we observed a weak reduction of infection by RRV gH-AELAAN by siRNA mediated knockdown of Plxdc2 expression, and comparatively potent and specific inhibition by one out of two rabbit antisera to Plxdc2.

The receptor-specificity conveyed by the respective interaction motif was further analyzed in lentiviral vector-mediated Plxdc1/2-Strep overexpression experiments in Raji B lymphocytes. EphA7 was used as control for Eph-mediated infection. Expression of Plxdc1/2-Strep as well as EphA7-Strep dramatically enhanced susceptibility of Raji cells (Fig 4D and 4E). RRV-YFP wt infection increased from  $0.14 \pm 0.04\%$  on empty vector transduced Raji cells to ~8.5% upon EphA7 overexpression and to ~17% upon Plxdc1/2 overexpression, without pronounced differences between the Plxdc family members. Mutation of the Eph-interaction motif in RRV-YFP gH-AELAAN completely abrogated the gain in susceptibility on EphA7 overexpressing cells while mutation of the Plxdc-interaction motif completely abrogated the gain in susceptibility on Plxdc1/2 overexpressing cells, confirming selective knockout of each individual receptor interaction in the respective mutant. Furthermore, deletion of the Eph-interaction motif in RRV-YFP gH-AELAAN did not impact the infection of Plxdc1/2 overexpressing cells in comparison to RRV-YFP wt infection. In contrast, we observed an ~2-fold higher infection of RRV-YFP gH $\Delta$ 21–27 on EphA7 overexpression cells, when compared to RRV-YFP wt. Together, the blocking and overexpression experiments indicate an independent rather than cooperative nature of Eph and Plxdc receptor function.

To quantitatively analyze the contribution of the Plxdc1/2-interaction to RRV infection of different cell types, RRV-YFP wt and RRV-YFP receptor binding mutant inocula were normalized to genome copies as determined by qPCR, and target cells were inoculated with the same number of encapsidated input virus genomes for wt and each mutant virus strain. At least three (four for SLK, HaCaT, Raji, MMB1845, five for MFB5487) independent sets of RRV wt and mutant stocks were used in infection experiments at various dilutions to compensate

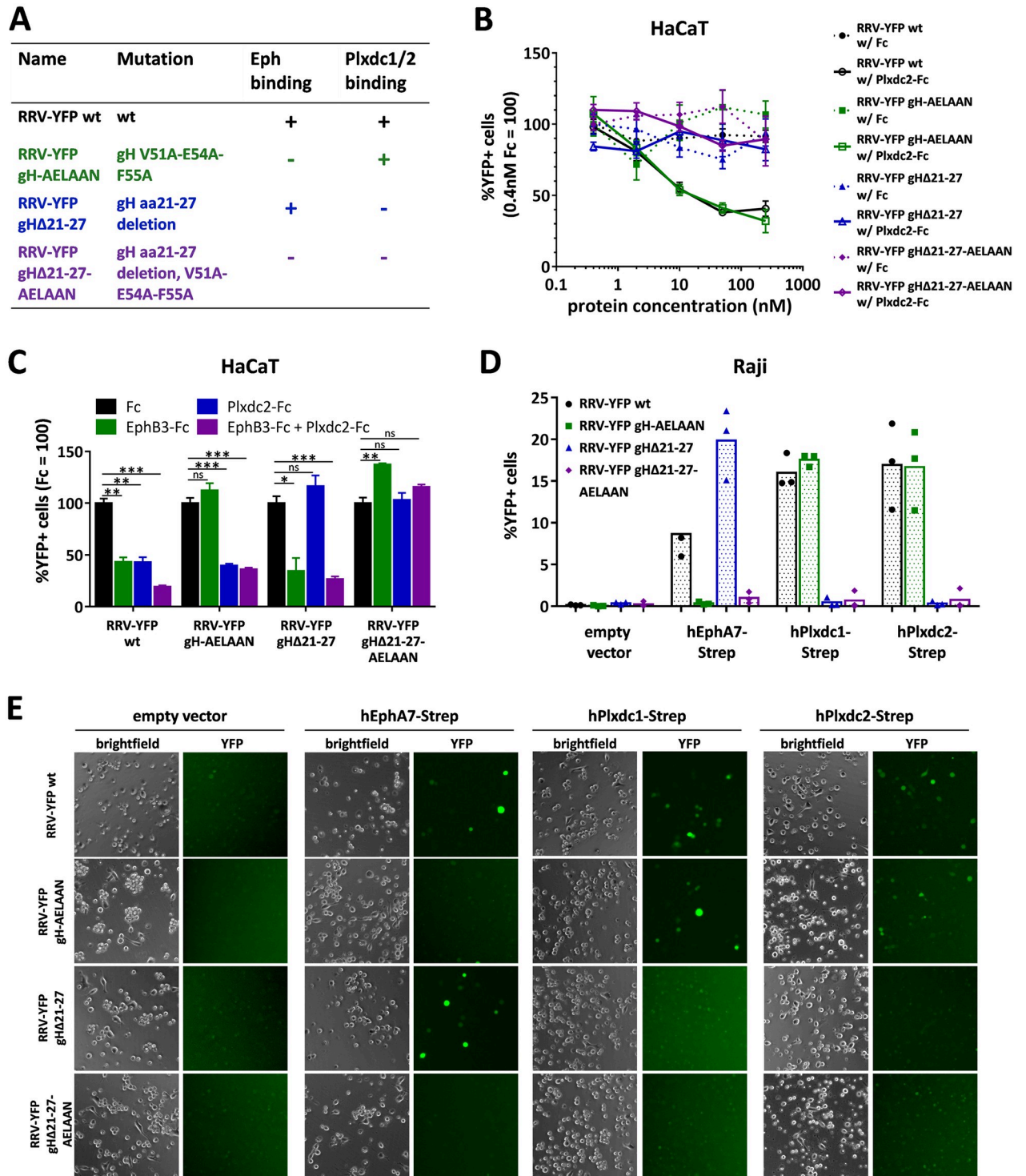


**Fig 4. Deletion of the seven amino acid Plxdc-binding motif is sufficient to detarget RRV 26–95 from Plxdc receptors.** A) List of BAC-derived recombinant viruses and introduced mutations used in this figure. B) Dose-dependent inhibition of RRV 26–95 infection by soluble human Plxdc2-FcStrep on HaCaT cells. RRV-YFP wt, RRV-YFP gH-AELAAN, RRV-YFP gHΔ21–27 and RRV-YFP gHΔ21-27-AELAAN were pre-incubated with hPlxdc2-FcStrep for 30min at room temperature. FcStrep alone was used as control. YFP expression as indicator of infection was measured by flow cytometry. Infection in the presence of 0.4nM FcStrep was set to 100% (MOI ~0.05, triplicates, error bars represent SD). C) Inhibition of RRV 26–95 infection by soluble Plxdc2-FcStrep and EphB3-Fc on HaCaT cells. RRV-YFP wt, RRV-YFP gH-AELAAN, RRV-YFP gHΔ21–27 and RRV-YFP gHΔ21-27-AELAAN were pre-incubated with 100nM hPlxdc2-FcStrep, 10nM EphB3-Fc or a combination of 100nM hPlxdc2-FcStrep and 10nM EphB3-Fc for 30min at room temperature. FcStrep alone was used as control. YFP expression as indicator of infection

was measured by flow cytometry. Infection with FcStrep was set to 100% (MOI ~0.1–0.2, triplicates, error bars represent SD). **D**) Raji cells were transduced with TwinStrep-tagged human EphA7, Plxdc1 or Plxdc2 (hEphA7-Strep/ hPlxdc1-Strep/ hPlxdc2-Strep) expression constructs or an empty vector control, briefly selected and infected with RRV-YFP wt, RRV-YFP gH-AELAAN, RRV-YFP gH $\Delta$ 21–27 or RRV-YFP gH $\Delta$ 21–27-AELAAN normalized to genome copies as determined by qPCR. YFP expression as indicator of infection was measured by flow cytometry. The mean across three independent sets of RRV stocks is indicated by columns. The means of individual triplicate infections for each set of RRV stocks are given as symbols within the respective columns. **E**) Micrographs show representative infection of one set of RRV stocks in (**D**).

<https://doi.org/10.1371/journal.ppat.1008979.g004>

for variability in stock preparation. For adherent cells, dilutions, which produced an RRV-YFP wt infection in an MOI range of 0.05 to 1 on the respective cell line, were chosen for further analysis. Infection as determined by the percentage of YFP+ cells was normalized to RRV-YFP wt, which was set to 1. For suspension cell lines, experiments with RRV-YFP wt infection over 1% were included in the analysis. None of the analyzed adherent cell lines showed a preferential use of Plxdc receptors over Eph receptors based on the reduction of specific infectivity of Eph-binding and Plxdc-interaction-deficient mutants (**Fig 5A**). Compared to RRV-YFP wt infection on rhesus monkey fibroblasts (RF), RRV-YFP gH $\Delta$ 21–27, RRV-YFP gH-AELAAN and RRV-YFP gH $\Delta$ 21–27-AELAAN exhibited a decrease in infection of ~30%, 50% and 70%, respectively. Similarly on HaCaT, infection with RRV-YFP gH-AELAAN and RRV-YFP gH $\Delta$ 21–27-AELAAN was reduced by ~60% and 75%, respectively, compared to RRV-YFP wt. While RRV-YFP gH $\Delta$ 21–27 exhibited a defect comparable to RRV-YFP gH-AELAAN in three of the analyzed independent sets of RRV stocks, this reduction in infectivity did not reach significance due to one outlier. In agreement with reduced infection of Eph- and Plxdc-binding virus mutants on HaCaT cells, *EPHB3* and *PLXDC2* expression was detected in HaCaT cells in published datasets (GSE95080, GSE138800) and by confirmatory qPCR of our samples (**S3A and S3B Fig**). On SLK cells, mutation of the Eph-interaction motif led to an ~65% decrease in infection, while RRV-YFP gH $\Delta$ 21–27 infection was on average comparable to RRV-YFP wt infection. In contrast, we identified B lymphocyte lines of human and macaque origin that exhibit a preference in the receptor usage for either Eph or Plxdc family members (**Fig 5B**). When normalized to genome copies, RRV-YFP gH $\Delta$ 21–27 infection on human Raji lymphoblasts was comparable to RRV-YFP wt infection while mutation of the Eph-interaction motif led to an ~90% decrease in infection, indicating preferential infection through Eph family receptors, albeit at low levels, as mentioned above. Correspondingly, with the exception of *EPHB4*, expression of all members of the Eph and Plxdc receptor families is low to absent in Raji cells, both in a published data set (GSE111880) and our subset analysis by qPCR (**S3C and S3D Fig**). Similar to Raji cells, RRV-YFP gH $\Delta$ 21–27 exhibited only a minor defect (~20% reduced infection) on immortalized B lymphocytes of *Macaca mulatta* origin (MMB1845) that did not reach significance, while infection with RRV-YFP gH-AELAAN and gH $\Delta$ 21–27-AELAAN was reduced by ~90% in comparison to RRV-YFP wt, again indicating preferential infection through Eph family receptors. Conversely, deletion of the Plxdc-interaction motif decreased infection of a B lymphocyte cell line of *Macaca fascicularis* origin (MFB5487) by ~75% whereas RRV-YFP gH-AELAAN exhibited an ~50% defect, indicating preferential use of the Plxdc interaction for infection of MFB5487 by RRV. This data fits with an expression analysis of *EPHA7*, *EPHB3*, *PLXDC1* and *PLXDC2* expression in Raji and MFB5487 cells which indicated comparatively high *PLXDC2* expression levels in MFB5487 cells (**S3D Fig**). Mutation of both the Eph- and Plxdc-interaction motif (RRV-YFP gH $\Delta$ 21–27-AELAAN) led to an even more pronounced defect of ~90% on MFB5487.

To evaluate the contribution of potential attachment effects on the observed differences in specific infectivity, we analyzed the capacity of virions to bind Plxdc1/2 overexpressing Raji cells in comparison to empty vector transduced Raji cells (**Fig 5C and 5D**). It should be noted that transduction with an Plxdc1 encoding lentiviral vector invariably resulted in higher levels

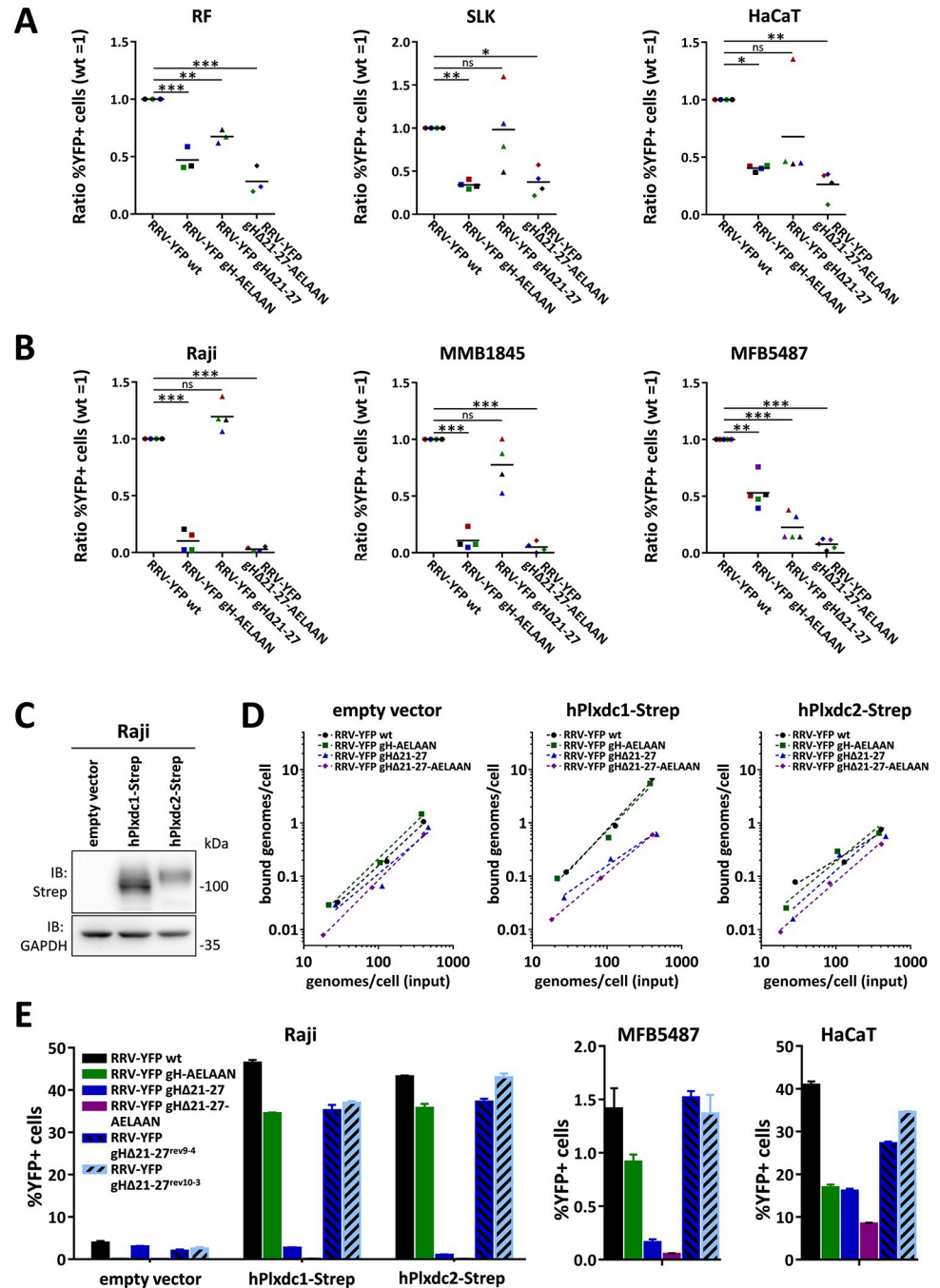


**Fig 5. The contribution of the RRV 26–95 gH-Plxdc interaction to infection is cell type-specific and may in part be dependent on attachment effects.** **A)** RRV 26–95 deleted in the Plxdc interaction motif exhibits reduced specific infectivity on HaCaT and RF, but not SLK cells. Target cells were infected with RRV-YFP wt, RRV-YFP gH-AELAAN, RRV-YFP gHΔ21–27 or RRV-YFP gHΔ21–27-AELAAN normalized to genome copies as determined by qPCR. YFP expression as indicator of infection was measured by flow cytometry and normalized to RRV-YFP wt infection. Means of individual normalized infections with three (RF) or four (HaCaT, SLK) independent sets of RRV stocks are given as symbols of different color. Sets with RRV-YFP wt infection in an MOI range of 0.05–1 were used for analysis. The mean across the independent sets of RRV stocks is indicated by black lines. **B)** RRV 26–95 deleted in the Plxdc interaction motif exhibits reduced specific infectivity on MFB5487, but not Raji and MMB1845 cells. Target cells were infected with RRV-YFP wt, RRV-YFP gH-AELAAN, RRV-YFP gHΔ21–27 or RRV-YFP gHΔ21–27-AELAAN normalized to genome copies as determined by qPCR. YFP expression as indicator of infection was measured by flow cytometry and normalized to RRV-YFP wt infection. Means of individual normalized infections with four (Raji,

MMB1845) or five (MFB5487) independent sets of RRV stocks are given as symbols of different color. Sets with RRV-YFP wt infection exceeding 1% were used for analysis. The maximal achieved RRV-YFP wt infection was 6.1% for Raji, 5.6% for MMB1845 and 3.1% for MFB5487, respectively. The mean across the independent sets of RRV stocks is indicated by black lines. **C)** Western blot analysis of Raji cells transduced with TwinStrep-tagged human Plxdc1 and Plxdc2 (hPlxdc1-Strep/ hPlxdc2-Strep) expression constructs or an empty vector control. **D)** Attachment of RRV 26–95 on transduced Raji cells is affected by hPlxdc1-Strep, but not hPlxdc2-Strep overexpression. Cells, analyzed in (C), were incubated with cold virus at the indicated concentrations at 4 °C for 30min followed by genomic DNA isolation. Bound genomes/cells as calculated based on qPCR of a genomic (CCR5) and a viral locus (ORF73/ LANA) were plotted against input viral genome number determined by ORF73/ LANA qPCR. **E)** Re-introduction of the seven amino acid motif crucial for Plxdc interaction rescues RRV-YFP gHΔ21–27 infection. Transduced Raji cells, MFB5487 and HaCaT cells were infected with RRV-YFP wt, RRV-YFP gH-AELAAN, RRV-YFP gHΔ21–27, RRV-YFP gHΔ21–27-AELAAN or two RRV-YFP gHΔ21–27 revertants (RRV-YFP gHΔ21–27<sup>rev9-4</sup>, RRV-YFPgHΔ21–27<sup>rev10-3</sup>) normalized to genome copies as determined by qPCR. YFP expression as indicator of infection was measured by flow cytometry (triplicates, error bars represent SD).

<https://doi.org/10.1371/journal.ppat.1008979.g005>

of protein expression as assessed by Western blot analysis than transduction with an Plxdc2 encoding lentiviral vector (Fig 5C). The number of bound viral DNA genomes/cell was used as a marker for virus attachment. Mutation of the Plxdc- and Eph-interaction motif had no clear effect on attachment to control vector-transduced and hPlxdc2-Strep-overexpressing Raji cells. In contrast, Raji cells overexpressing hPlxdc1-Strep showed increased attachment of RRV-YFP wt and RRV-YFP gH-AELAAN, while attachment of Plxdc-interaction negative RRV-YFP mutants gHΔ21–27 and gHΔ21–27-AELAAN was not enhanced and remained comparable to empty vector control and hPlxdc2-Strep-overexpressing cells.

To exclude effects of potential offsite genomic rearrangements in RRV-YFP gHΔ21–27 we created two independent revertants (RRV-YFP gHΔ21–27<sup>rev9-4</sup> and RRV-YFP gHΔ21–27<sup>rev10-3</sup>). Restoration of the residues deleted in RRV-YFP gHΔ21–27 restored infection on hPlxdc1/2-transduced Raji, MFB5487 and HaCaT cells to RRV-YFP wt levels, with no pronounced differences between RRV-YFP wt, RRV-YFP gHΔ21–27<sup>rev9-4</sup> and RRV-YFP gHΔ21–27<sup>rev10-3</sup> (Fig 5E). Similar to the ~11-fold increase of RRV-YFP wt infection upon hPlxdc1/2 overexpression, infection with RRV-YFP gHΔ21–27 revertants increased from 2.00% ± 0.30% (2.54% ± 0.29%) on empty vector transduced Raji cells to 35.3% ± 1.21% (37.0% ± 0.39%) and 37.3% ± 0.68% (43.0% ± 0.99%) upon hPlxdc1 and hPlxdc2 overexpression for RRV-YFP gHΔ21–27<sup>rev9-4</sup> (RRV-YFP gHΔ21–27<sup>rev10-3</sup>), respectively (Fig 5E).

Our interaction data (Fig 1A and 1B) suggests that at least RRV 26–95 gH can bind Plxdc1/2 in the absence of gL. We therefore aimed to analyze if infection with a RRV 26–95 gL deletion mutant (RRV-YFP ΔgL) is influenced by Plxdc1 and 2 expression to a similar degree as RRV-YFP wt and RRV-YFP gH-AELAAN infection. As shown before, overexpression of hEphA7-Strep or hPlxdc1-Strep in Raji cells dramatically increased RRV-YFP wt infection compared to empty vector transduced cells (22-fold for hEphA7-Strep, 23-fold for hPlxdc1-Strep and 26-fold for hPlxdc2-Strep) (Fig 6A and 6B and S4 Fig). RRV-YFP gH-AELAAN infection was increased from 0.25% ± 0.05% basal infection on empty vector transduced cells to 52.5% ± 2.06% and 65.5% ± 1.22%, respectively, upon hPlxdc1-Strep or hPlxdc2-Strep overexpression, while hEphA7-Strep overexpression had no pronounced effect on infection. We observed a pattern similar to RRV-YFP gH-AELAAN for the infection with two independent RRV-YFP ΔgL clones, RRV-YFP ΔgL<sup>3-3</sup> and RRV-YFP ΔgL<sup>3-5</sup>. While hEphA7-Strep overexpression did not influence RRV-YFP ΔgL infection, hPlxdc1/2-Strep overexpression enhanced infection from 0.36% ± 0.03% (0.48% ± 0.04%) on empty vector transduced Raji cells to 31.1% ± 0.95% (36.3% ± 1.42%) and 35.6% ± 0.94% (42.6% ± 0.57%) upon hPlxdc1 and hPlxdc2 overexpression for RRV-YFP ΔgL<sup>3-3</sup> (RRV-YFP ΔgL<sup>3-5</sup>), respectively (Fig 6B). Even though the effect of Plxdc1/2 overexpression on RRV-YFP ΔgL infection was slightly less pronounced than the effect on RRV-YFP wt and RRV-YFP gH-AELAAN

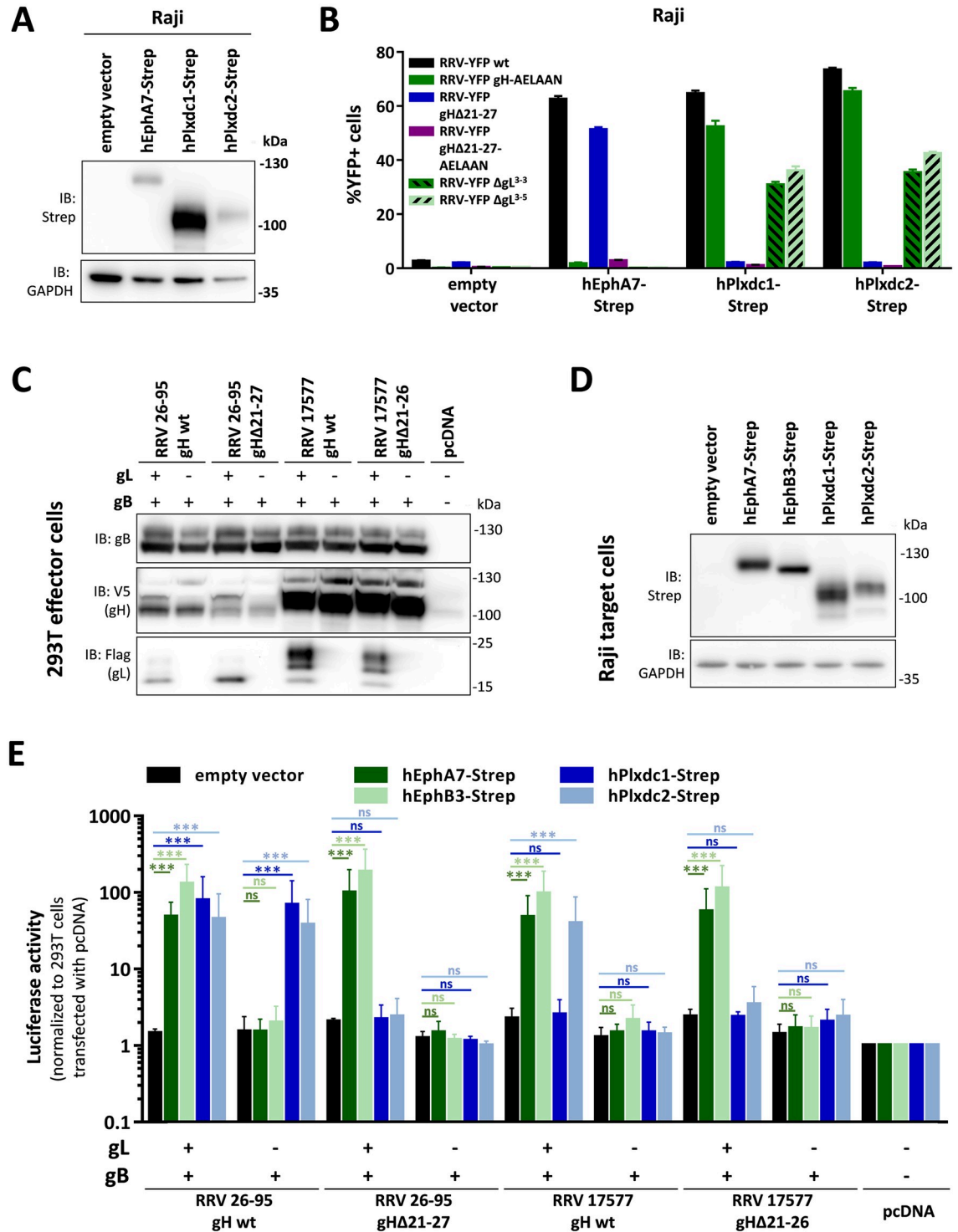


**Fig 6. Plxdc1/2-dependent infection with RRV 26-95 does not require gL.** **A)** Raji cells were transfected with TwinStrep-tagged human EphA7, Plxdc1 and Plxdc2 (hEphA7-Strep/ hPlxdc1-Strep/ hPlxdc2-Strep) expression constructs or an empty vector control and briefly selected by antibiotic resistance. Lysates of transfected Raji cell pools were analyzed for EphA7-Strep and Plxdc1/2-Strep expression by Western blot. **B)** Transduced Raji cells analyzed in (A) were infected with RRV-YFP wt, RRV-YFP gH-AELAAN, RRV-YFP gHA21-27 or one of two RRV-YFP ΔgL clones normalized to genome copies as determined by qPCR. YFP expression as indicator of infection was measured by flow cytometry (triplicates, error bars represent SD). **C-E)** Cell-cell fusion assay: Transfected 293T effector cells were co-cultured with transfected Raji target cells as indicated. Cell-cell fusion was assessed after two days of co-culture. Protein expression of 293T effector cells transfected with empty vector or the indicated viral glycoprotein combinations (C) or

of transduced Raji target cells (D) was analyzed by Western blot. Expression controls were harvested directly prior to the start of co-culture. Luciferase activity as indicator of cell-cell fusion was measured after 48h of effector and target cell co-culture (E). Luciferase activity is normalized to empty vector transfected 293T effector cells (n = 3, error bars represent SD).

<https://doi.org/10.1371/journal.ppat.1008979.g006>

infection, this data demonstrates that the use of Plxdc1 and Plxdc2 as RRV 26–95 entry receptors is possible in a gL-independent manner.

Our data indicating that Plxdc-mediated RRV entry is gL-independent is interesting as the gH/gL/gB complex is widely regarded as the conserved herpesviral core fusion machinery [21]. Therefore, we sought to determine if cell-cell fusion mediated by RRV glycoproteins is similarly influenced by Plxdc1 and Plxdc2 in an gL-independent manner. We established a quantitative fusion assay using 293T cells transfected with a VP16-Gal4 transcription factor construct as effector cells and Raji cells transduced with a lentivirus encoding a Gal4-response element-driven luciferase construct as target cells (Raji-Gal4-Luc). 293T cells were co-transfected with viral glycoproteins gH, gL and gB as indicated while stable Raji-Gal4-Luc cells were transduced with lentiviral vectors encoding TwinStrep-tagged human receptor constructs. In addition to Plxdc1 and Plxdc2, EphA7 and the high-affinity RRV receptor EphB3 were used as controls for gL-dependent receptor interaction of gH (Fig 6C and 6D). Luciferase activity as indicator of cell-cell fusion was measured after two days of effector-target cell co-culture (Fig 6E). Compared to the baseline of control transfected 293T cells, fusion activity was increased 79-fold and 45-fold in 293T cells expressing the full RRV 26–95 gH/gL/gB complex when co-cultured with Raji-Gal4-Luc cells expressing Plxdc1-Strep and Plxdc2-Strep, respectively. The luciferase activity was not markedly altered in the absence of RRV 26–95 gL. In contrast, fusion activity of RRV 17577 glycoprotein expressing cells was only significantly enhanced (~18-fold) over Raji-Gal4-Luc empty vector cells in Plxdc2-Strep but not Plxdc1-Strep transduced target cells. For both, RRV 26–95 and RRV 17577, deletion of the Plxdc-interaction motif in gH (RRV 26–95 gH $\Delta$ 21–27/ RRV 17577 gH $\Delta$ 21–26) reversed the Plxdc-mediated fusion activity both in the presence and absence of gL. Cell-cell fusion with hEphA7-Strep or hEphB3-Strep expressing cells was only facilitated by expression of the full gH/gL/gB fusion machinery in effector cells. Expression of RRV 26–95 gH/gL/gB or RRV 26–95 gH $\Delta$ 21–27/gL/gB lead to a 48-fold (129-fold) or 100-fold (185-fold) enhanced luciferase activity in co-culture experiments using hEphA7-Strep (hEphB3-Strep) overexpressing Raji cells, while expression of RRV 26–95 gH/gB or RRV 26–95 gH $\Delta$ 21–27/gB did not significantly enhance luciferase activity over background in the same setting. Similarly, fusion of hEphA7-Strep or hEphB3-Strep overexpressing Raji cells with RRV 17577 glycoprotein expressing cells was only significantly increased over background in the presence of gL (~50-fold for EphA7-expressing cells and ~100-fold for EphB3-expressing cells compared to control transfected 293T cells). This data demonstrates that RRV 26–95 gH/gB but not RRV 17577 gH/gB can induce cell-cell fusion independent of gL upon interaction with Plxdc receptors.

## Discussion

In this study we identified the Plexin domain containing proteins 1 and 2 as a novel family of entry receptors for RRV. Plxdc1/2 interact with the gH/gL complex of RRV in a region close to the previously characterized binding motif for Eph receptors. While the Eph-interaction as well as the critical Eph binding motif in domain I of gH is conserved between RRV and the closely related human pathogenic KSHV [23], the interaction with Plxdc1/2 is exclusive to RRV and even exhibits differences between isolates 26–95 and 17577 as prototypic members of the two described RRV sequence clades.

According to our results, differences between Plxdc1 and Plxdc2 may also exist in terms of function. While overexpression of both Plxdc1 and Plxdc2 in Raji cells, that were virtually “non-susceptible” under the conditions used, lead to robust RRV 26–95 infection (Fig 4D and 4E), only overexpression of Plxdc1 enhanced attachment of RRV wt and RRV gH-AELAAN in comparison to either non-transduced Raji cells or Plxdc-binding deficient RRV mutants (Fig 5D). Whether this is primarily due to differences in expression levels, consistently observed between Plxdc1 and Plxdc2 upon lentiviral overexpression or due to underlying functional differences in the gH interaction with these molecules remains to be determined.

Mutation of residues Tyr23 and Glu25 in gH domain I, which are conserved between RRV isolate 26–95 and 17577, almost abolished the interaction with Plxdc2, which is bound by gH/gL of both isolates. Although the same residues are critical for the interaction of RRV gH 26–95 with Plxdc1, the partial conservation of the region appears to be insufficient to confer binding of 17577 gH to Plxdc1. Interestingly, the interaction of 17577 gH with Plxdc2 is dependent on the presence of gL in the gH/gL complex, whereas 26–95 gH is able to bind Plxdc1/2 independently of gL. This interaction data was corroborated by functional analysis of Plxdc-mediated RRV 26–95 and RRV 17577 infection and fusion. As shown above, RRV 26–95 infection was enhanced by both Plxdc1 and Plxdc2 expression (Fig 2E and 2H) and similarly RRV 26–95 gH/gL or gH alone facilitated fusion with Plxdc1 or Plxdc2 overexpressing Raji cells (Fig 6E). In contrast, recombinant overexpression of Plxdc2, but not of Plxdc1 enhanced infection with RRV 17577 (Fig 2F and 2I), which was paralleled in our fusion assay: RRV 17577 gH/gB/gL effector cells fused readily with Plxdc2 overexpressing target cells, but not in the absence of gL or with Plxdc1 overexpressing target cells (Fig 6E). These features of Plxdc1/2 binding specificities appear similar to the interaction of the gH/gL complex with Eph receptors, wherein mutation of the strictly conserved Eph interaction motif is sufficient to abrogate receptor binding, but differences in KSHV and RRV affinities for A- and B-type Eph RTKs indicate the existence of additional regions in gH or gL that contribute to or modulate the interaction, which is corroborated by a recent crystal structure of KSHV gH/gL in complex with EphA2 [36]. Whether these preferences for different members of conserved receptor families also influence e.g. cell or tissue tropism, viral spread or pathogenicity has not been determined. Sequence comparisons of over twenty RRV isolates identified dramatic differences in the extracellular domains of gH (58.7% amino acid identity between phylogenetic groups) as well as in gL (54.4% amino acid identity between phylogenetic groups) between isolates that fell in two discrete groupings either similar to 26–95 or 17577, while variation in other glycoproteins R1, gM, gN, orf68 was minimal between clades [4]. However, if these clade-specific glycoprotein variations influence the observed differences in pathogenicity between RRV strains 26–95 and 17577 remains to be seen, but such differences have been reported for the representative isolates (summarized in [37]). An interesting coincidence is that the primary sequence of Japanese macaque rhadinovirus (JMRV) [38] gH is highly similar to that of RRV 26–95 with 96% amino acid identity, highly suggestive of conservation of the Plxdc interaction. This virus was found associated with encephalomyelitis in macaques [39], and Plexin domain containing proteins are expressed in brain ([28] and <https://www.proteinatlas.org/>), supporting the notion of a certain neurotropism of RV2 rhadinoviruses. Another interesting question would be if the receptor-binding function of the N-terminal region of gH is conserved between RRV and KSHV, and probably EBV, and whether KSHV and EBV can bind another receptor through this region. So far, we did not identify corresponding interactions for KSHV, but in principle the region of gH encompassing the Plxdc2 binding site is present in both viruses and it is tempting to assume some functional conservation.

Along those lines, the evolutionary factors that drive interaction with different receptor families and the resulting multitude of herpesvirus–receptor interactions is highly interesting. For e.g. EBV and HCMV, a clear correlation between receptor usage, dependent on viral

interaction partners of the gH/gL complex, and cell tropism has been demonstrated in various studies ([40], reviewed in [41]). However, for rhadinoviruses, the picture is less clear. We demonstrated that RRV infection of select cell lines exhibits a dependence on specific receptors, e.g. Raji infection—to the modest extent that was possible without recombinant receptor over-expression—was dependent on the gH/gL-Eph interaction, while MFB5487 infection was more dependent on the Plxdc-interaction (Fig 5B). Additionally, mutation of the Eph-interaction motif did not impact infection on all cell types equivalently [23]. Although the complexity and partial redundancy of the RRV interaction with different members of the Eph and Plxdc receptor family complicates the inference of direct correlations between receptor expression and infection, expression data of select Eph receptors in comparison to Plxdc is in line with the observed receptor preferences on different cell types (S3 Fig). Yet, a definite correlation between exclusive receptor usage and infection of specific cell types is not obviously apparent. While the notion of a role of different receptor interactions in KSHV and RRV cell and tissue tropism is tempting and an established concept for related viruses [41–43], the possibility of a redundant function should not be discarded. Redundancy could be driven by the need to escape antibodies e.g. to one receptor binding site. For instance, *in vitro* infection of human keratinocytes or rhesus monkey fibroblasts seemed to be impacted to a similar degree by either deletion of the Eph- or of the Plxdc-interaction motif (Fig 5). To ultimately address the correlation between receptor- and tissue-tropism, *in vivo* studies using receptor-de-targeted mutants to analyze cell and tissue tropisms will be required. The importance of *in vivo* studies is also supported by a recent report that showed that a gL-null RRV mutant still established persistent infection in the B cell compartment upon intravenous inoculation, while infection of B cells *in vitro* was drastically reduced [24], a finding that could be explained by the gL-independent usage of Plxdc1/2 for B cell infection *in vivo*. At a minimum, our data on RRV-YFP  $\Delta$ gL infection of Plxdc1 and Plxdc2 overexpressing Raji cells (Fig 6B) confirms that RRV can efficiently use Plxdc1 and Plxdc2 as entry receptors in the absence of gL.

Finally, the fact that a mutant that was deleted in both the Eph and the Plxdc1/2 interaction motif, RRV-YFP gH $\Delta$ 21-27-AELAAN, was still able to replicate on rhesus monkey fibroblasts, as evidenced by the fact that we were able to grow a virus stock on these cells, and was still infectious to a certain degree on a number of cell lines (Figs 4 and 5) indicates a surprisingly high degree of redundancy in the entry pathways that RRV can use and hints at the existence of additional receptors or host factors besides Ephs and Plexin domain containing proteins.

On a more speculative note, the apparent overlap between virus receptors and tumor-associated membrane proteins may represent an interesting research subject. Eph receptors were first identified in an attempt to characterize tyrosine kinases involved in cancer [44] and altered expression in various cancer types has been demonstrated for several Eph family members (reviewed in [45]). Similarly, Plxdc1 was first described in a screen for novel tumor endothelial members [25] and expression of both Plxdc1 and Plxdc2 is elevated in the endothelium of solid tumors [25,26,46,47]. Plxdc1 expression has been described as prognostic marker and modulating factor for various human cancers [46–50]. Given the overlap between the required changes e.g. in metabolism, transcription, and signaling for cancer growth and virus replication it seems not unlikely that either elevated expression or signaling of these molecules is favorable for both virus infection and cancer progression.

## Material and methods

### Cells

Human embryonic kidney (HEK) 293T cells (RRID:CVCL\_0063) (laboratory of Tobias Moser), SLK cells (RRID:CVCL\_9569) (NIH AIDS Research and Reference Reagent program), rhesus

monkey fibroblasts (RF) (laboratory of Prof. Rüdiger Behr) and HaCaT human keratinocytes (RRID:CVCL\_0038) were cultured in Dulbecco's Modified Eagle Medium (DMEM), high glucose, GlutaMAX, 25mM HEPES (Thermo Fisher Scientific) supplemented with 10% fetal calf serum (FCS) (Thermo Fisher Scientific), and 50 $\mu$ g/ml gentamycin (PAN Biotech). iSLK cells (laboratory of Don Ganem, Novartis Institutes for BioMedical Research, Emeryville, CA, USA) were maintained in DMEM supplemented with 10% FCS, 50 $\mu$ g/ml gentamycin, 2.5 $\mu$ g/ml puromycin (InvivoGen) and 250 $\mu$ g/ml G418 (Carl Roth). Raji cells (RRID:CVCL\_0511) (laboratory of Jens Gruber), MFB5487 (a clonal cell line established from *Macaca fascicularis* PBMC, immortalized by infection with herpesvirus papio; a kind gift from Ulrike Sauermann) and MMB1845 cells (a clonal cell line established from *Macaca mulatta* PBMC, immortalized by infection with herpesvirus papio; a kind gift from Ulrike Sauermann) were cultured in RPMI (Thermo Fisher Scientific) supplemented with 10% FCS and 50 $\mu$ g/ml gentamycin.

### BAC mutagenesis and virus production

RRV recombinants (RRV-YFP gH $\Delta$ 21–27, RRV-YFP  $\Delta$ gL and RRV-YFP gH $\Delta$ 21–27-AELAAN) were generated based on BAC35-8 [51] and RRV gH-AELAAN [23] respectively, using a two-step, markerless  $\lambda$ -red-mediated BAC recombination strategy as described by Tischer et al. [35]. RRV-YFP  $\Delta$ gL harbors a 128 bp deletion, which introduces a frameshift after amino acid 26 and a stop codon after amino acid 37, leaving only six amino acids of the original gL sequence after the putative signal peptide cleavage site. RRV-YFP gH $\Delta$ 21–27 revertants were generated based on RRV-YFP gH $\Delta$ 21–27 following the same protocol described by Tischer et al. [35]. In short, recombination cassettes were generated from the pEPKanS template by polymerase chain reaction (PCR) with Phusion High Fidelity DNA polymerase (Thermo Fisher Scientific) using long oligonucleotides (Ultramers; purchased from Integrated DNA Technologies (IDT)) (see S2 Table for a complete list of primers). Recombination cassettes were transformed into RRV-YFP-carrying GS1783 followed by kanamycin selection, and subsequent second recombination under 1% L(+)-arabinose (Sigma-Aldrich)-induced I-SceI expression. RRV-YFP 17577 was generated by shuttling the RRV 26–95 CMV-YFP expression cassette flanked by overhangs identical in RRV 26–95 and RRV 17577 into an RRV 17577 wt bacmid (a kind gift from Scott W. Wong). Recombination cassettes were transformed into RRV 17577-carrying GS1783 and recombination was performed as described above. Colonies were verified by PCR of the mutated region followed by sequence analysis (Macrogen), pulsed-field gel electrophoresis and restriction fragment length polymorphism. For this purpose, bacmid DNA was isolated by standard alkaline lysis from 5ml liquid cultures. Subsequently, the integrity of bacmid DNA was analyzed by digestion with restriction enzyme *Xho*I and separation in 1% PFGE agarose (Bio-Rad) gels and 0.5 $\times$ TBE buffer by pulsed-field gel electrophoresis at 6 V/cm, 120-degree field angle, switch time linearly ramped from 1s to 5s over 16 h (CHEF DR III, Bio-Rad). Infectious RRV-YFP recombinants were generated as described previously [23]. In short, bacmid DNA (NucleoBond Xtra Midi) was transfected into 293T cells using GenJet Ver. II (Signagen) according to manufacturer's instructions. Transfected 293T cells were transferred onto a confluent rhesus monkey fibroblasts monolayer two days after transfection and co-cultivated until a visible cytopathic effect (CPE) was observed. For virus stock preparations, confluent primary rhesus monkey fibroblasts were inoculated with infectious supernatant of 293T/rhesus monkey fibroblast co-cultures. After multiple rounds of replication, virus-containing RF supernatant was clarified by centrifugation (4750g, 10min), concentrated by overnight centrifugation (4200rpm, 4°C) and careful aspiration of approximately 95% of the supernatant. The pellet was resuspended overnight in the remaining liquid. Stocks of wt and recombinant viruses were aliquoted and stored at -80°C.

Mutations were verified by PCR amplification of the respective region followed by sequence analysis (Macrogen). (See [S2 Table](#) for a complete list of primers and constructs).

## Plasmids

The pcDNA4 vector containing full-length *EPHB3* (ref|BC052968|, pcDNA-EphB3-myc), pcDNA6aV5 vectors containing RRV/KSHV gH and gL coding sequences (ref|GQ994935.1|, pcDNA6aV5-KSHV-gH, pcDNA3.1-KSHV-gL-Flag [14]; ref|AF210726.1|, pcDNA6aV5-RRV-26-95-gH, pcDNA3.1-RRV-26-95-gL-Flag [15,52]; ref|AF083501.3|, pcDNA6aV5-RRV-17577-gH, pcDNA3.1-RRV-17577-gL-Flag [15]) were described elsewhere. RRV 26-95/ RRV 17577 recombinant gH constructs were generated based on pcDNA6aV5-RRV-26-95-gH or pcDNA6aV5-RRV-17577-gH, respectively, using 'Round the Horn' Site-directed mutagenesis. Expression plasmids pcDNA4-hPlxdc1-myc (*Homo sapiens*, full-length, ref|NM\_020405.5|) and pcDNA4-hPlxdc2-myc (*Homo sapiens*, full-length, ref|NM\_032812.9|) were generated by PCR based restriction cloning. The coding sequence of the soluble ectodomain of human Plxdc2 (amino acids 31–453) without signal peptide was inserted behind a heterologous signal peptide of murine IgG-kappa into pAB61Strep by PCR-based restriction cloning, resulting in a C-terminally fused IgG1 Fc-fusion protein with a C-terminal tandem Strep-Tag (pPlxdc2-FcS) as described previously [53]. pcDNA6 vectors constructs containing the coding sequence of the human Plxdc1 ectodomain (aa 1–425) with a 6XHis Tag (pcDNA6-ectoPlxdc1-6XHis) or the coding sequence of the human Plxdc2 ectodomain (aa 1–453) with a 6XHis Tag (pcDNA6-ectoPlxdc2-6XHis) were based on pcDNA4-hPlxdc1-myc/ pcDNA4-hPlxdc2-myc, which were PCR-amplified and ligated using exonuclease-based Gibson-assembly (Gibson Assembly Mastermix, New England Biolabs). Expression plasmids pcDNA4-mmPlxdc1-myc (*Macaca mulatta*, full-length, ref|XM\_028836436.1|) and pcDNAmPlxdc2-myc (*Macaca mulatta*, full-length, ref|XM\_028826043.1|) were generated based on PCR-amplified gBlock gene fragments (purchased from IDT) of the regions varying from human *PLXDC1* (nt1-1200) and *PLXDC2* (nt1-1401), respectively, and ligated in the respective PCR-amplified backbone (pcDNA4-hPlxdc1-myc, pcDNA4-hPlxdc2-myc) by exonuclease-based Gibson-assembly. pLenti CMV Blast DEST (706–1) (a gift from Eric Campeau & Paul Kaufman (Addgene plasmid #17451)) constructs carrying a human Plxdc1-TwinStrep or Plxdc2-TwinStrep expression cassette (pLenti-CMV-Blast-Plxdc1-Strep/ pLenti-CMV-Blast-Plxdc2-Strep) were based on pcDNA4-hPlxdc1-myc/ pcDNA4-hPlxdc2-myc, which were PCR-amplified and ligated using exonuclease-based Gibson-assembly. pLenti-CMV-Blast-EphA7-Strep was described before [20]. RRV 26-95/ RRV 17577 recombinant gB constructs were generated by inserting gB coding sequences which were PCR-amplified from RRV-YFP 26–95 (MN488839.2) or RRV-YFP 17577 bacmid DNA in PCR-amplified pcDNA4-myc backbone by exonuclease-based Gibson-assembly. This resulted in full-length gB expression constructs (pcDNA4-RRV26-95-gB, pcDNA4-RRV17577-gB) followed by a short amino acid sequence (LEGPSNKNSSQKRI). The lentiviral construct encoding a Gal4 response element driven TurboGFP-luciferase reporter gene was generated by transferring the complete Gal4-TurboGFP-luciferase cassette described before [54] into the PCR-amplified pLenti CMV Blast DEST (706–1) backbone. The Gal4 DNA binding domain VP16 fusion plasmid was described before [54]. (See [S2 Table](#) for a complete list of primers and constructs).

## Recombinant proteins

Recombinant, soluble FcStrep and Plxdc2-FcStrep-fusion proteins were purified under native conditions by Strep-Tactin chromatography from 293T cell culture supernatant. 293T cells were transfected using Polyethylenimine "Max" (PEI) (Polysciences) [55] as described before

[20] with pAB61Strep or pPlxdc2-FcS. The protein-containing cell culture supernatant was filtered through 0.22 $\mu$ m PES membranes (Millipore) and passed over 0.5ml of a Strep-Tactin Superflow (IBA Lifesciences) matrix in a gravity flow Ominiprep column (BioRad). Bound protein was washed with approximately 50ml phosphate buffered saline pH 7.4 (PBS) and eluted in 1ml fractions with 3mM desthiobiotin (Sigma-Aldrich) in PBS. Recombinant Plxcd1 ectodomain or Plxdc2 ectodomain protein was purified under native conditions by Ni-NTA chromatography from 293T cell culture supernatant. 293T cells were transfected with pcDNA6-ectoPlxdc1-6XHis or pcDNA6-ectoPlxdc2-6XHis using PEI transfection. The protein-containing cell culture supernatant was filtered through 0.22 $\mu$ m PES membranes (Millipore), concentrated using VIVAFLOW 50R (Sartorius) and passed over 1ml of a Ni-NTA Agarose (Macherey-Nagel) matrix in a gravity flow Ominiprep column (BioRad). Bound protein was washed with approximately 50ml TBS (150mM NaCl, 50mM Tris-HCl, pH 7.6) and eluted in 1ml fractions with 500 mM Imidazole in TBS. Protein-containing fractions were pooled, concentrated via VivaSpin columns (Sartorius) and applied over Äkta Avant (GE) on a HiPrep 16/60 Sephacryl S300HR column (GE). For all recombinant proteins, protein-containing fractions were pooled and buffer exchange to PBS via VivaSpin columns (Sartorius) was performed. Protein concentration was determined by absorbance at 280nm. Aliquots were frozen and stored at  $-80^{\circ}$ C. Recombinant, human, soluble EphB3-Fc (5667-B3-050) was purchased from R&D Systems.

### Lentivirus production and transduction

For production of lentiviral particles, 10cm cell culture grade petri dishes of approximately 80% confluent 293T cells were transfected with 1.4 $\mu$ g pMD2.G (VSV-G envelope expressing plasmid, a gift from Didier Trono (Addgene plasmid #12259), 3.6 $\mu$ g psPAX2 (Gag-Pol expression construct, a gift from Didier Trono (Addgene plasmid #12260), and 5 $\mu$ g of lentiviral expression constructs (pLenti CMV Blast DEST (706-1), pLenti-CMV-Blast-EphA7-Strep, pLenti-CMV-Blast-Plxdc1-Strep, pLenti-CMV-Blast-Plxdc2-Strep) using PEI as described before [20]. The supernatant containing the pseudotyped lentiviral particles was harvested 2 to 3 days after transfection and filtered through 0.45 $\mu$ m CA membranes (Millipore). For transduction, lentivirus stocks were used at a 1:5 dilution unless stated otherwise. After 48h, the selection antibiotic blasticidin (Invivogen) was added to a final concentration of 10 $\mu$ g/ml. After initial selection the blasticidin concentration was reduced to 5 $\mu$ g/ml.

### Real-time PCR (qPCR) analysis of *EPH* and *PLXDC* gene expression

For analysis of *EPHA7*, *EPHB3*, *PLXDC1* and *PLXDC2* expression by qPCR,  $1 \times 10^6$  cells were harvested in RNAzol (Thermo Fisher) and RNA was isolated using the Direct-zol RNA Mini-prep Plus Kit (Zymo) according to the manufacturer's instructions. 1 $\mu$ g total RNA was used for cDNA synthesis using the SensiFAST cDNA Synthesis Kit (Bioline) according to manufacturer's instructions. qPCR was performed on a StepOne Plus cyler (Thermo Fisher Scientific) in 20 $\mu$ l reactions using the SensiFAST SYBR Hi-ROX Kit (Bioline) (cycling conditions: 2min initial denaturation at  $95^{\circ}$ C, 40 cycles:  $95^{\circ}$ C for 5s and  $65^{\circ}$ C for 25s). Relative expression was calculated based on  $\Delta$ Ct to *GAPDH*. Samples were analyzed in technical triplicates, only samples with amplification in all triplicates were scored as positive. See [S2 Table](#) for a complete list of primers.

### Real-time PCR (qPCR)-based viral genome copy number analysis and virus attachment assay

Concentrated virus samples were treated with DNaseI (0.1 units/ $\mu$ l) to remove any non-encapsidated DNA ( $37^{\circ}$ C, overnight). Subsequently, DNaseI was inactivated and viral capsids

were disrupted by heating the samples to 95°C for 30min. qPCR was performed on a StepOne Plus cycler in 20µl reactions using the SensiFAST Probe Hi-ROX Kit (Bioline) (cycling conditions: 3min initial denaturation at 95°C, 40 cycles 95°C for 10s and 60°C for 35s). All primer-probe sets were purchased from IDT as complete PrimeTime qPCR Assays (primer:probe ratio = 4:1). Samples were analyzed in technical triplicates. A series of five 10-fold dilutions of bacmid DNA was used as standard for absolute quantification of viral genome copies based on qPCR of RRV ORF73. For virus attachment assays transduced Raji cells were incubated with ice-cold virus dilutions at the indicated concentrations, normalized to genomes per cell, at 4°C for 30min. After three washes with ice-cold PBS genomic DNA was isolated using the ISOLATE II Genomic DNA Kit (Bioline) according to manufacturer's instructions. Genome copies of used input virus preparations were determined after overnight DNaseI digest as described above. qPCR was performed as described above using primer-probe sets specific for RRV ORF73 and a cellular genomic locus (CCR5). Viral copy numbers were determined based on a 10-fold dilution series of bacmid DNA, while cell numbers were calculated based on a 2-fold dilution series of Raji gDNA. For attachment assays all samples were analyzed in technical duplicates. See [S2 Table](#) for a complete list of primers.

### siRNA-mediated knock-down

For siRNA-mediated knock-down of Plxdc2, 293T cells were plated one day prior to transfection in 6well plates. 10µl of a 5µM siRNA solution (set of 4x siCtrl or set of 4x siPlxdc2) purchased as ON-TARGETplus siRNAs from Dharmacon were transfected using 2µl of DharmaFECT 1 transfection reagent (Dharmacon) according to manufacturer's instructions in serum-free DMEM without antibiotics. 6h post transfection fresh DMEM supplemented with 20% FCS was added to achieve a final concentration of 10%FCS. 48h post transfection 293T siCtrl cells and 293T siPlxdc2 cells were harvested, cell numbers were determined and cells were plated at 50 000 cells/cm<sup>2</sup> for infection assays (see below). For determination of knock-down efficiency, cells were harvested in RNazol 96h post transfection and RNA was isolated using the Direct-zol RNA Miniprep Plus Kit according to the manufacturer's instructions. qPCR was performed on a StepOne Plus cycler (Thermo Fisher Scientific) in 20µl reactions with 40ng RNA/reaction using the SensiFAST Probe Hi-ROX One-Step Kit (Bioline) (cycling conditions: 10min 45°Cmin, 2min initial denaturation at 95°C, 40 cycles 95°C for 5s and 60°C for 20s). Primer-probe sets specific for Plxdc2 and GAPDH were used. Samples were analyzed in technical triplicates. See [S2 Table](#) for a complete list of primers.

### Infection assays, blocking experiments and flow cytometry

For infection assays cells were plated at 50 000 cells/cm<sup>2</sup> (SLK, HaCaT, 293T), 25 000 cells/cm<sup>2</sup> (RF) or 200 000 cells/ml (Raji, MFB5487, MMB1845) respectively. One day after plating (for adherent cells lines) or directly after plating (for suspension cell lines), cells were infected with the indicated amounts of virus. Adherent cells lines were harvested 24h post infection by brief trypsinization, followed by addition of 5% FCS in PBS to inhibit trypsin activity. Suspension cell lines were harvested 48h post infection (24h post infection for transduced Raji cells) by pipetting. Subsequently, cells were pelleted by centrifugation (1200rpm, 10min), washed once with PBS, re-pelleted and fixed in PBS supplemented with 4% formaldehyde (Carl Roth). Block of RRV infection with soluble decoy receptor was assayed by infection with virus inocula that were pre-incubated with the indicated concentrations of soluble EphB3-Fc, hPlxdc1-FcStrep, hPlxdc2-FcStrep or FcStrep alone at room temperature for 30min. Calculation of molarity was based on dimeric proteins. For blocking assays using anti-Plxdc2 antibodies, custom rabbit immune sera raised against recombinant Plxdc2-FcStrep (Eurogentec) were used.

293T cells, were pre-treated with an 1:5 dilution of Plxdc2 immune serum or pre-immune serum of the respective animal in DMEM supplemented with 10% FCS for 30min at 37°C. After pre-incubation virus was added in 1/5<sup>th</sup> of the total incubation volume per well. Cell harvest and preparation for flow cytometry analyses was performed as described above. A minimum of 5 000–10 000 cells was analyzed per sample for YFP expression on a LSRII flow cytometer (BD Biosciences). Data was analyzed using Flowing Software (Version 2.5).

### Immunoprecipitation and Western blot analysis

Affinity-purification of gH-interacting proteins using gH-FcStrep was performed as described previously [15]. Protein bands were visualized after PAGE on 8–16% gradient gels by silver staining using the SilverQuest Silver Staining Kit (Thermo Fisher Scientific), cut out using a scalpel, destained, and sent to the Taplin Mass Spectrometry Facility, Harvard Medical School, for analysis. For interaction analysis of gH-V5/gL-Flag complexes with Plxdc1/2, 293T cells were transfected using PEI as described before. Lysates of 293T cells transfected with the respective expression constructs for gH-V5/gL-Flag complexes were prepared in NP40 lysis buffer (1% Nonidet P40 Substitute (Sigma-Aldrich), 150mM NaCl (Sigma-Aldrich), 50mM HEPES (VWR), 1mM EDTA (Amresco) with freshly added Protease Inhibitor Cocktail, General Use (Amresco)) and protein content was determined by Bradford assay using Roti-Quant (Roth) according to manufacturer's instructions. 20µg total protein was denatured in 1x SDS sample buffer (Morris formulation) at 95°C for 5min, separated by polyacrylamide gel electrophoresis (PAGE) using 8–16% Tris-Glycine polyacrylamide gradient gels (Thermo Fisher Scientific) with Tris-Glycine SDS running buffer (25mM Tris, 192mM glycine, 0.1% SDS) and transferred to 0.45µm (0.22µm for blots containing gL) Polyvinylidene difluoride (PVDF) membranes (200mA/Gel, max 30V, 1h in Towbin buffer (25mM Tris, 192mM glycine) with 20% methanol) in a wet tank system (Mini Blot Module, Thermo Fisher). The membranes were blocked in 5% dry milk powder in TBS-T (5mM Tris, 15mM NaCl, 0.05% Tween20) for 1h, at room temperature, washed once in TBS-T and incubated with the respective antibodies for 2h at room temperature or overnight at 4°C (see S2 Table for a complete list of antibodies). After three washes with TBS-T, the membranes were incubated with the respective HRP-conjugated secondary antibody in 5% dry milk powder in TBS-T for 1h at room temperature washed three times in TBS-T and imaged on an ECL ChemoCam 3.2 Imager (Intas) using Immobilon Forte Western HRP substrate (Merck Millipore). For pulldown of gH-V5 or gH-V5/gL-Flag complexes, the amount of input lysate between wt and mutant gH constructs was normalized to gH expression as determined by Western blot and diluted to equal volume with cell lysate from non-transfected 293T cells prior to immunoprecipitation. Subsequently, lysates were incubated with 0.5µg V5-tag antibody (Bio-Rad) and ProteinG sepharose (GenScript) overnight at 4°C with agitation. After three washes in NP40 lysis buffer, ProteinG beads with pre-coupled complexes were incubated overnight at 4°C with agitation with lysate of full-length human or *Macaca mulatta* Plxdc1-myc or Plxdc2-myc expression plasmid transfected 293T cells normalized to Plxdc expression. Volumes were adjusted with lysate from untransfected 293T cells. ProteinG beads were collected by brief centrifugation and washed 3 times in NP40 lysis buffer. Precipitates were heated in 2x SDS sample buffer (95°C, 5min) and analyzed by Western blot as described above. For co-immunoprecipitation of soluble Plxdc1/2-Strep constructs with gH-V5/gL-Flag and EphB3-myc, supernatant of Plxdc1/2-FcStrep transfected 293T cells was incubated with StrepTactinXT beads (IBA) overnight at 4°C with agitation. After three washes in NP40 lysis buffer, StrepTactinXT beads with pre-coupled Plxdc1/2-FcStrep were incubated overnight at 4°C with agitation with equal amounts of lysate of full-length human EphB3-myc, RRV 26–95 gH-V5/gL-Flag or 17577 gH-V5/gL-Flag expression

plasmid transfected 293T cells or the indicated combinations. Volumes were adjusted with lysate of untransfected 293T cells.

### Enzyme-linked immunosorbent assay (ELISA)

F96 Maxisorp Nunc-Immuno Plates (Thermo Fisher Scientific) were coated with recombinant RRV 26–95 gH-FcStrep/gL (described previously [15]) at 1 µg/ml in PBS overnight. After three washes with PBS-T, the wells were blocked with 10% FBS in PBS for 2h. Incubation with Plxdc1 ectodomain or Plxdc2 ectodomain was performed for 2h at room temperature in 10% FBS in PBS. The plates were washed three times with PBS-T. Bound protein was detected via the C-terminal 6XHis Tag using 6XHis Antibody MA1-135 (Invitrogen) followed by three washes in TBS-T and incubation with donkey anti-mouse horseradish peroxidase (HRP)-coupled secondary antibody (Dianova). After three washes, 3,3',5,5'-Tetramethylbenzidine (TMB) substrate (Thermo Fisher Scientific) was added and the reaction was stopped by adding 1M HCl. The plates were imaged on a Biotek Synergy 2 plate reader.

### Fusion assay

On day1, Raji effector cells stably transduced with a lentiviral construct encoding a Gal4 response element driven TurboGFP-luciferase reporter (Raji-Gal4-Luc) were transduced with lentiviruses encoding TwinStrep-tagged human receptor constructs or an empty vector control. 293T cells were seeded in 96-well plates at 30 000 cells/well. On day2, 293T target cells were transfected with a plasmid encoding the Gal4 DNA binding domain fused to the VP16 transactivator (VP16-Gal4) and the indicated viral glycoprotein combinations or a pcDNA control (VP16-Gal4: 31.25ng/well, gH: 12.5ng/well, gL (pcDNA in gH/gB only combinations): 62.5ng/well, gB: 18.75ng/well, pcDNA only: 93.75ng/well) using PEI as described before. 24h after transfection, medium on 293T target cells was completely removed and exchanged to 100 µl fresh DMEM supplemented with 10% FCS and 50 µg/ml gentamycin. Transduced Raji cells were counted, cells were pelleted, resuspended in fresh DMEM supplemented with 10% FCS and 50 µg/ml gentamycin and 40 000 Raji cells transduced with receptor constructs or an empty vector control were added to 293T target cells in 50 µl full medium. Triplicate wells were used for all target-effector combinations. After 48h, cells were washed once in PBS and lysed in 35 µl 1x Luciferase Cell culture lysis buffer (E1531, Promega) for 15min at room temperature and centrifuged for 10min at 4°C. 20 µl of each cell lysate were used to measure luciferase activity using the Beetle-Juice Luciferase Assay according to manufacturer's instructions on a Biotek Synergy 2 plate reader.

### Structure prediction and analysis

Homology based structure prediction was performed using the Iterative Threading ASSEMBLY Refinement (I-TASSER) server on standard settings for structure prediction of RRV 26–95 gH and gL based on the crystal structure of the EBV gH/gL complex (3PHF). Modeling of the RRV 26–95 gH/gL complex was additionally performed using both the SPRING and CO-THreader algorithms for protein-protein complex structure and multi-chain protein threading with no differences between determined structures. Resulting I-TASSER structures were aligned to the gH/gL CO-THreader model with the VMD 1.9.3 OpenGL RMSD Trajectory Tool based on amino acids 25 to 62 of gH (RMSD of 0.344 Å) and amino acids 2 to 100 of gL (RMSD of 2.697 Å) to generate the depicted model. All further analyses and visualizations were performed using VMD 1.9.3 OpenGL.

## Mathematical and statistical analysis

Statistical difference between groups was determined by unpaired Student's t-tests followed by Bonferroni correction for multiple comparisons or by ordinary one-way (Fig 2I) or two-way (Fig 2H and S2C and S2D Fig) analysis of variance (ANOVA) followed by Dunnett's correction for multiple comparisons. Statistical analysis for Fig 6E, presented on a logarithmical scale, was performed on log-transformed normalized data using a repeated measures two-way ANOVA followed by Dunnett's correction for multiple comparisons. All Statistical analyses were performed with GraphPad Prism version 6. For all statistics, \*: p-value < 0.05, \*\*: p-value < 0.01, \*\*\*: p-value < 0.001, ns: not significant.

## Supporting information

**S1 Fig. *EPH* and *PLXDC* expression in 293T cells and *Plxdc1/2* alignment showing the domain junctions.** A) Normalized read counts of the 14 *EPH* receptor genes, *PLXDC1* and *PLXDC2* as found in the GEO data set series GSE153744 (HEK 293T DMSO rep1-4, GSM4652564, GSM4652566, GSM4652568, GSM4652569) and GSE156152 (Mock-1-3, GSM4725672, GSM4725673, GSM4725674). B) Expression of selected *EPH* genes, *PLXDC1* and *PLXDC2* analyzed by qPCR in 293T cells. C) Alignment of human (hs) and rhesus macaque (mm) *Plxdc1* and *Plxdc2*. Junctions of domains (blue letters and lines) and the putative transmembrane domain (blue box) as described by Cheng et al. [31] are indicated. (TIF)

**S2 Fig. siRNA-mediated knock-down of *PLXDC2* as well as immune serum raised against recombinant *Plxdc2* reduce RRV infection.** A-C) 293T cells were treated with siRNA against *PLXDC2* (si*Plxdc2*) or control siRNA (siCtrl) for 72h. *PLXDC2* expression was assessed using qPCR (A). Values were normalized to *GAPDH* expression and are shown relative to siCtrl. The cells were infected with RRV-YFP wt or mutants as indicated (B). YFP expression as indicator of infection was measured by flow cytometry. Infection was normalized to infection of siCtrl treated 293T cells. The mean relative infection of two sets of RRV stocks in two dilutions is shown. Absolute infection rates of 293T siCtrl cells for all stocks and dilutions are given as % YFP+ cells in C. D-F) 293T cells were pre-incubated with rabbit serum raised against recombinant *Plxdc2* (two animals: SY8512, SY8513) or pre-immune serum (PPI) of the same animals for 30min prior to infection with RRV-YFP wt or the indicated mutants. YFP expression as indicator of infection was measured by flow cytometry (triplicates, error bars represent SD). Absolute infection rates of 293T cells treated with pre-immune serum are given as %YFP+ cells in F. (TIF)

**S3 Fig. *EPH* and *PLXDC* expression in HaCaT, Raji, MFB5487, RF and MMB1845 cells.** A) Normalized read counts of the 14 *EPH* receptor genes, *PLXDC1* and *PLXDC2* as found in the GEO data set series GSE138800 (C1-C3, GSM4119632, GSM4119633, GSM4119634) and GSE95080 (Uninfected HaCaT, GSM2495796). B) Expression of selected *EPH* genes, *PLXDC1* and *PLXDC2* analyzed by qPCR in HaCaT cells. C) Normalized read counts of the 14 *EPH* receptor genes, *PLXDC1* and *PLXDC2* as found in the GEO data set series GSE111880 (Raji total RNA (replicate1-4), GSM3043273, GSM3043274, GSM3043275, GSM3043276). D) Expression of selected *EPH* genes, *PLXDC1* and *PLXDC2* analyzed by qPCR in Raji and MFB5487 cells. E) Expression of selected *EPH* genes, *PLXDC1* and *PLXDC2* analyzed by qPCR in RF and MMB1845 cells. (TIF)

**S4 Fig. Plxdc1/2-dependent infection with RRV 26–95 does not require gL.** Raji cells were transduced with TwinStrep-tagged human EphA7, Plxdc1 and Plxdc2 (hEphA7-Strep/hPlxdc1-Strep/hPlxdc2-Strep) expression constructs or an empty vector control, briefly selected and infected with RRV-YFP wt, RRV-YFP gH-AELAAN, RRV-YFP gH $\Delta$ 21–27, RRV-YFP gH $\Delta$ 21-27-AELAAN or one of two RRV-YFP  $\Delta$ gL clones normalized to genome copies as determined by qPCR. Micrographs show representative infection of the indicated cell pools.

(TIF)

**S1 Table. List of peptides identified by LC-MS/MS.**

(XLSX)

**S2 Table. List of primers and antibodies used in this study.**

(XLSX)

## Acknowledgments

We thank Scott W. Wong (Oregon Health & Science University) for kindly providing anti-RRV gB (3H8.1) antibody.

## Author Contributions

**Conceptualization:** Anna K. Großkopf, Alexander S. Hahn.

**Data curation:** Armin Ensser.

**Formal analysis:** Anna K. Großkopf, Armin Ensser, Alexander S. Hahn.

**Funding acquisition:** Ronald C. Desrosiers, Alexander S. Hahn.

**Investigation:** Anna K. Großkopf, Sarah Schlagowski, Thomas Fricke, Armin Ensser, Alexander S. Hahn.

**Methodology:** Anna K. Großkopf, Thomas Fricke, Alexander S. Hahn.

**Project administration:** Alexander S. Hahn.

**Resources:** Alexander S. Hahn.

**Supervision:** Ronald C. Desrosiers, Alexander S. Hahn.

**Validation:** Armin Ensser.

**Visualization:** Anna K. Großkopf.

**Writing – original draft:** Anna K. Großkopf.

**Writing – review & editing:** Anna K. Großkopf, Sarah Schlagowski, Alexander S. Hahn.

## References

1. Desrosiers RC, Sasseville VG, Czajak SC, Zhang X, Mansfield KG, Kaur A, et al. A herpesvirus of rhesus monkeys related to the human Kaposi's sarcoma-associated herpesvirus. *J Virol.* 1997; 71: 9764–9769. <https://doi.org/10.1128/JVI.71.12.9764-9769.1997> PMID: 9371642
2. Searles RP, Bergquam EP, Axthelm MK, Wong SW. Sequence and genomic analysis of a Rhesus macaque rhadinovirus with similarity to Kaposi's sarcoma-associated herpesvirus/human herpesvirus 8. *J Virol.* 1999; 73: 3040–3053. <https://doi.org/10.1128/JVI.73.4.3040-3053.1999> PMID: 10074154
3. O'Connor CM, Kedes DH. Rhesus Monkey Rhadinovirus: A Model for the Study of KSHV. In: Boshoff C, Weiss RA, editors. *Kaposi Sarcoma Herpesvirus: New Perspectives.* Springer Berlin Heidelberg; 2007. pp. 43–69.

4. Shin YC, Jones LR, Manrique J, Lauer W, Carville A, Mansfield KG, et al. Glycoprotein gene sequence variation in rhesus monkey rhadinovirus. *Virology*. 2010; 400: 175–186. <https://doi.org/10.1016/j.virol.2010.01.030> PMID: 20172576
5. Bilello JP, Morgan JS, Damania B, Lang SM, Desrosiers RC. A Genetic System for Rhesus Monkey Rhadinovirus: Use of Recombinant Virus To Quantitate Antibody-Mediated Neutralization. *J Virol*. 2006; 80: 1549–1562. <https://doi.org/10.1128/JVI.80.3.1549-1562.2006> PMID: 16415030
6. Estep RD, Powers MF, Yen BK, Li H, Wong SW. Construction of an Infectious Rhesus Rhadinovirus Bacterial Artificial Chromosome for the Analysis of Kaposi's Sarcoma-Associated Herpesvirus-Related Disease Development. *J Virol*. 2007; 81: 2957–2969. <https://doi.org/10.1128/JVI.01997-06> PMID: 17215283
7. Bilello JP, Lang SM, Wang F, Aster JC, Desrosiers RC. Infection and Persistence of Rhesus Monkey Rhadinovirus in Immortalized B-Cell Lines. *J Virol*. 2006; 80: 3644–3649. <https://doi.org/10.1128/JVI.80.7.3644-3649.2006> PMID: 16537632
8. Wong SW, Bergquam EP, Swanson RM, Lee FW, Shiigi SM, Avery NA, et al. Induction of B cell hyperplasia in simian immunodeficiency virus-infected rhesus macaques with the simian homologue of Kaposi's sarcoma-associated herpesvirus. *J Exp Med*. 1999; 190: 827–840. <https://doi.org/10.1084/jem.190.6.827> PMID: 10499921
9. Orzechowska BU, Powers MF, Sprague J, Li H, Yen B, Searles RP, et al. Rhesus macaque rhadinovirus-associated non-Hodgkin lymphoma: animal model for KSHV-associated malignancies. *Blood*. 2008; 112: 4227–4234. <https://doi.org/10.1182/blood-2008-04-151498> PMID: 18757778
10. Bruce AG, Bielefeldt-Ohmann H, Barcy S, Bakke AM, Lewis P, Tsai C-C, et al. Macaque Homologs of EBV and KSHV Show Uniquely Different Associations with Simian AIDS-related Lymphomas. Gao S-J, editor. *PLoS Pathog*. 2012; 8: e1002962. <https://doi.org/10.1371/journal.ppat.1002962> PMID: 23055934
11. Marshall VA, Labo N, Hao X-P, Holdridge B, Thompson M, Miley W, et al. Gammaherpesvirus infection and malignant disease in rhesus macaques experimentally infected with SIV or SHIV. Dittmer DP, editor. *PLOS Pathog*. 2018; 14: e1007130. <https://doi.org/10.1371/journal.ppat.1007130> PMID: 30001436
12. Umbach JL, Strelow LI, Wong SW, Cullen BR. Analysis of rhesus rhadinovirus microRNAs expressed in virus-induced tumors from infected rhesus macaques. *Virology*. 2010; 405: 592–599. <https://doi.org/10.1016/j.virol.2010.06.036> PMID: 20655562
13. Ensser A, Yasuda K, Lauer W, Desrosiers RC, Hahn AS. Rhesus Monkey Rhadinovirus Isolated from Hemangioma Tissue. *Microbiol Resour Announc*. 2020; 9. <https://doi.org/10.1128/MRA.01347-19> PMID: 32193241
14. Hahn AS, Kaufmann JK, Wies E, Naschberger E, Panteleev-Ivlev J, Schmidt K, et al. The ephrin receptor tyrosine kinase A2 is a cellular receptor for Kaposi's sarcoma-associated herpesvirus. *Nat Med*. 2012; 18: 961–966. <https://doi.org/10.1038/nm.2805> PMID: 22635007
15. Hahn AS, Desrosiers RC. Rhesus Monkey Rhadinovirus Uses Eph Family Receptors for Entry into B Cells and Endothelial Cells but Not Fibroblasts. Gao S-J, editor. *PLoS Pathog*. 2013; 9: e1003360. <https://doi.org/10.1371/journal.ppat.1003360> PMID: 23696734
16. TerBush AA, Hafkamp F, Lee HJ, Coscoy L. A Kaposi's Sarcoma-Associated Herpesvirus Infection Mechanism Is Independent of Integrins  $\alpha 3 \beta 1$ ,  $\alpha V \beta 3$ , and  $\alpha V \beta 5$ . Jung JU, editor. *J Virol*. 2018; 92: e00803–18. <https://doi.org/10.1128/JVI.00803-18> PMID: 29899108
17. Chen J, Zhang X, Schaller S, Jardetzky TS, Longnecker R. Ephrin Receptor A4 is a New Kaposi's Sarcoma-Associated Herpesvirus Virus Entry Receptor. Shenk T, editor. *mBio*. 2019; 10: e02892–18. <https://doi.org/10.1128/mBio.02892-18> PMID: 30782663
18. Hahn AS, Desrosiers RC. Binding of the Kaposi's sarcoma-associated herpesvirus to the ephrin binding surface of the EphA2 receptor and its inhibition by a small molecule. *J Virol*. 2014; 88: 8724–8734. <https://doi.org/10.1128/JVI.01392-14> PMID: 24899181
19. Kumar B, Chandran B. KSHV Entry and Trafficking in Target Cells—Hijacking of Cell Signal Pathways, Actin and Membrane Dynamics. *Viruses*. 2016; 8. <https://doi.org/10.3390/v8110305> PMID: 27854239
20. Großkopf AK, Schlagowski S, Hörnich BF, Fricke T, Desrosiers RC, Hahn AS. EphA7 Functions as Receptor on BJAB Cells for Cell-to-Cell Transmission of the Kaposi's Sarcoma-Associated Herpesvirus and for Cell-Free Infection by the Related Rhesus Monkey Rhadinovirus. Jung JU, editor. *J Virol*. 2019; 93: e00064–19. <https://doi.org/10.1128/JVI.00064-19> PMID: 31118261
21. Möhl BS, Chen J, Longnecker R. Gammaherpesvirus entry and fusion: A tale how two human pathogenic viruses enter their host cells. *Advances in Virus Research*. Elsevier; 2019. pp. 313–343. <https://doi.org/10.1016/bs.avir.2019.05.006> PMID: 31439152
22. TerBush AA, Hafkamp F, Lee HJ, Coscoy L. A Kaposi's Sarcoma-Associated Herpesvirus Infection Mechanism is Independent of Integrins  $\alpha 3 \beta 1$ ,  $\alpha V \beta 3$ , and  $\alpha V \beta 5$ . *J Virol*. 2018. <https://doi.org/10.1128/JVI.00803-18> PMID: 29899108

23. Großkopf AK, Ensser A, Neipel F, Jungnickl D, Schlagowski S, Desrosiers RC, et al. A conserved Eph family receptor-binding motif on the gH/gL complex of Kaposi's sarcoma-associated herpesvirus and rhesus monkey rhadinovirus. Hutt-Fletcher L, editor. *PLOS Pathog.* 2018; 14: e1006912. <https://doi.org/10.1371/journal.ppat.1006912> PMID: 29432452
24. Hahn AS, Bischof GF, Großkopf AK, Shin YC, Domingues A, Gonzalez-Nieto L, et al. A Recombinant Rhesus Monkey Rhadinovirus Deleted of Glycoprotein L Establishes Persistent Infection of Rhesus Macaques and Elicits Conventional T Cell Responses. *J Virol.* 2019; JVI.01093-19, jvi;JVI.01093-19v1. <https://doi.org/10.1128/JVI.01093-19> PMID: 31645449
25. St Croix B. Genes Expressed in Human Tumor Endothelium. *Science.* 2000; 289: 1197–1202. <https://doi.org/10.1126/science.289.5482.1197> PMID: 10947988
26. Carson-Walter EB, Watkins DN, Nanda A, Vogelstein B, Kinzler KW, St Croix B. Cell surface tumor endothelial markers are conserved in mice and humans. *Cancer Res.* 2001; 61: 6649–6655. PMID: 11559528
27. Miller-Delaney SFC, Lieberam I, Murphy P, Mitchell KJ. Plxdc2 is a mitogen for neural progenitors. *PLoS One.* 2011; 6: e14565. <https://doi.org/10.1371/journal.pone.0014565> PMID: 21283688
28. Lee HK, Bae HR, Park HK, Seo IA, Lee EY, Suh DJ, et al. Cloning, characterization and neuronal expression profiles of tumor endothelial marker 7 in the rat brain. *Brain Res Mol Brain Res.* 2005; 136: 189–198. <https://doi.org/10.1016/j.molbrainres.2005.02.010> PMID: 15893603
29. Miller SFC, Summerhurst K, Rünker AE, Kerjan G, Friedel RH, Chédotal A, et al. Expression of Plxdc2/TEM7R in the developing nervous system of the mouse. *Gene Expr Patterns GEP.* 2007; 7: 635–644. <https://doi.org/10.1016/j.modgep.2006.12.002> PMID: 17280871
30. Nanda A, Buckhaults P, Seaman S, Agrawal N, Boutin P, Shankara S, et al. Identification of a Binding Partner for the Endothelial Cell Surface Proteins TEM7 and TEM7R. *Cancer Res.* 2004; 64: 8507–8511. <https://doi.org/10.1158/0008-5472.CAN-04-2716> PMID: 15574754
31. Cheng G, Zhong M, Kawaguchi R, Kassai M, Al-Ubaidi M, Deng J, et al. Identification of PLXDC1 and PLXDC2 as the transmembrane receptors for the multifunctional factor PEDF. *eLife.* 2014; 3: e05401. <https://doi.org/10.7554/eLife.05401> PMID: 25535841
32. Lee HK, Seo IA, Park HK, Park HT. Identification of the basement membrane protein nidogen as a candidate ligand for tumor endothelial marker 7 in vitro and in vivo. *FEBS Lett.* 2006; 580: 2253–2257. <https://doi.org/10.1016/j.febslet.2006.03.033> PMID: 16574105
33. Uhlen M, Fagerberg L, Hallstrom BM, Lindskog C, Oksvold P, Mardinoglu A, et al. Tissue-based map of the human proteome. *Science.* 2015; 347: 1260419–1260419. <https://doi.org/10.1126/science.1260419> PMID: 25613900
34. Matsuura H, Kirschner AN, Longnecker R, Jardetzky TS. Crystal structure of the Epstein-Barr virus (EBV) glycoprotein H/glycoprotein L (gH/gL) complex. *Proc Natl Acad Sci.* 2010; 107: 22641–22646. <https://doi.org/10.1073/pnas.1011806108> PMID: 21149717
35. Tischer BK, Smith GA, Osterrieder N. En Passant Mutagenesis: A Two Step Markerless Red Recombination System. In: Braman J, editor. *In Vitro Mutagenesis Protocols.* Totowa, NJ: Humana Press; 2010. pp. 421–430.
36. Su C, Wu L, Chai Y, Qi J, Tan S, Gao GF, et al. Molecular basis of EphA2 recognition by gHgL from gammaherpesviruses. *Nat Commun.* 2020; 11: 5964. <https://doi.org/10.1038/s41467-020-19617-9> PMID: 33235207
37. Estep RD, Wong SW. Rhesus macaque rhadinovirus-associated disease. *Curr Opin Virol.* 2013; 3: 245–250. <https://doi.org/10.1016/j.coviro.2013.05.016> PMID: 23747119
38. Estep RD, Hansen SG, Rogers KS, Axthelm MK, Wong SW. Genomic characterization of Japanese macaque rhadinovirus, a novel herpesvirus isolated from a nonhuman primate with a spontaneous inflammatory demyelinating disease. *J Virol.* 2013; 87: 512–523. <https://doi.org/10.1128/JVI.02194-12> PMID: 23097433
39. Axthelm MK, Bourdette DN, Marracci GH, Su W, Mullaney ET, Manoharan M, et al. Japanese macaque encephalomyelitis: A spontaneous multiple sclerosis-like disease in a nonhuman primate. *Ann Neurol.* 2011; 70: 362–373. <https://doi.org/10.1002/ana.22449> PMID: 21674589
40. Li Q, Turk SM, Hutt-Fletcher LM. The Epstein-Barr virus (EBV) BZLF2 gene product associates with the gH and gL homologs of EBV and carries an epitope critical to infection of B cells but not of epithelial cells. *J Virol.* 1995; 69: 3987–3994. <https://doi.org/10.1128/JVI.69.7.3987-3994.1995> PMID: 7539502
41. Nguyen C, Kamil J. Pathogen at the Gates: Human Cytomegalovirus Entry and Cell Tropism. *Viruses.* 2018; 10: 704. <https://doi.org/10.3390/v10120704> PMID: 30544948
42. Wang X, Kenyon WJ, Li Q, Müllberg J, Hutt-Fletcher LM. Epstein-Barr Virus Uses Different Complexes of Glycoproteins gH and gL To Infect B Lymphocytes and Epithelial Cells. *J Virol.* 1998; 72: 5552–5558. <https://doi.org/10.1128/JVI.72.7.5552-5558.1998> PMID: 9621012

43. Chen J, Sathiyamoorthy K, Zhang X, Schaller S, Perez White BE, Jardetzky TS, et al. Ephrin receptor A2 is a functional entry receptor for Epstein-Barr virus. *Nat Microbiol*. 2018. <https://doi.org/10.1038/s41564-017-0081-7> PMID: 29292384
44. Hirai H, Maru Y, Hagiwara K, Nishida J, Takaku F. A novel putative tyrosine kinase receptor encoded by the eph gene. *Science*. 1987; 238: 1717–1720. <https://doi.org/10.1126/science.2825356> PMID: 2825356
45. Pasquale EB. Eph receptors and ephrins in cancer: bidirectional signalling and beyond. *Nat Rev Cancer*. 2010; 10: 165–180. <https://doi.org/10.1038/nrc2806> PMID: 20179713
46. Zhang Z-Z, Hua R, Zhang J-F, Zhao W-Y, Zhao E-H, Tu L, et al. TEM7 (PLXDC1), a key prognostic predictor for resectable gastric cancer, promotes cancer cell migration and invasion. *Am J Cancer Res*. 2015; 5: 772–781. PMID: 25973314
47. Carpenter RL, Paw I, Zhu H, Sirkisoon S, Xing F, Watabe K, et al. The gain-of-function GLI1 transcription factor TGLI1 enhances expression of VEGF-C and TEM7 to promote glioblastoma angiogenesis. *Oncotarget*. 2015; 6: 22653–22665. <https://doi.org/10.18632/oncotarget.4248> PMID: 26093087
48. Czekierdowski A, Stachowicz N, Czekierdowska S, Łoziński T, Gurynowicz G, Kluz T. Prognostic significance of TEM7 and nestin expression in women with advanced high grade serous ovarian cancer. *Ginekol Pol*. 2018; 89: 135–141. <https://doi.org/10.5603/GP.a2018.0023> PMID: 29664548
49. Kim GH, Won JE, Byeon Y, Kim MG, Wi TI, Lee JM, et al. Selective delivery of PLXDC1 small interfering RNA to endothelial cells for anti-angiogenesis tumor therapy using CD44-targeted chitosan nanoparticles for epithelial ovarian cancer. *Drug Deliv*. 2018; 25: 1394–1402. <https://doi.org/10.1080/10717544.2018.1480672> PMID: 29890852
50. Falchetti ML, D'Alessandris QG, Pacioni S, Buccarelli M, Morgante L, Giannetti S, et al. Glioblastoma endothelium drives bevacizumab-induced infiltrative growth via modulation of PLXDC1. *Int J Cancer*. 2019; 144: 1331–1344. <https://doi.org/10.1002/ijc.31983> PMID: 30414187
51. Hahn AS, Großkopf AK, Jungnickl D, Scholz B, Ensser A. Viral FGARAT Homolog ORF75 of Rhesus Monkey Rhadinovirus Effects Proteasomal Degradation of the ND10 Components SP100 and PML. Jung JU, editor. *J Virol*. 2016; 90: 8013–8028. <https://doi.org/10.1128/JVI.01181-16> PMID: 27356898
52. Shin YC, Desrosiers RC. Rhesus Monkey Rhadinovirus ORF57 Induces gH and gL Glycoprotein Expression through Posttranscriptional Accumulation of Target mRNAs. *J Virol*. 2011; 85: 7810–7817. <https://doi.org/10.1128/JVI.00493-11> PMID: 21613403
53. Hahn A, Birkmann A, Wies E, Dorer D, Mahr K, Sturzl M, et al. Kaposi's Sarcoma-Associated Herpesvirus gH/gL: Glycoprotein Export and Interaction with Cellular Receptors. *J Virol*. 2009; 83: 396–407. <https://doi.org/10.1128/JVI.01170-08> PMID: 18945775
54. Hörnich BF, Großkopf AK, Schlagowski S, Tenbusch M, Kleine-Weber H, Neipel F, et al. SARS-CoV-2 and SARS-CoV spike-mediated cell-cell fusion differ in the requirements for receptor expression and proteolytic activation. *Microbiology*; 2020 Jul. <https://doi.org/10.1101/2020.07.25.221135>
55. Longo PA, Kavran JM, Kim M-S, Leahy DJ. Transient Mammalian Cell Transfection with Polyethylenimine (PEI). *Methods in Enzymology*. Elsevier; 2013. pp. 227–240.